ISSN 0973-3302

THE JOURNAL OF ACOUSTICAL SOCIETY OF INDIA

Volume 52 Number 2 April 2025

A Quarterly Publication of the ASI
https://acoustics.org.in

The Journal of Acoustical Society of India
Volume 52 Number 2 April 2025 pp 42-77

ASI

The Journal of Acoustical Society of India

The Refereed Journal of the Acoustical Society of India (JASI)

The Journal of Acoustical Society of India is a refereed journal of the Acoustical Society of India **(ASI)**. The **ASI** is a non-profit national society founded in 31st July, 1971. The primary objective of the society is to advance the science of acoustics by creating an organization that is responsive to the needs of scientists and engineers concerned with acoustics problems all around the world.

Manuscripts of articles, technical notes and letter to the editor should be submitted to the Chief Editor. Copies of articles on specific topics listed above should also be submitted to the respective Associate Scientific Editor. Manuscripts are refereed by at least two referees and are reviewed by Publication Committee (all editors) before acceptance. On acceptance, revised articles with the text and figures scanned as separate files on a diskette should be submitted to the Editor by express mail. Manuscripts of articles must be prepared in strict accordance with the author instructions.

All information concerning subscription, new books, journals, conferences, etc. should be submitted to Chief Editor:

B. Chakraborty, CSIR - National Institute of Oceanography, Dona Paula, Goa-403 004,
Tel: +91.832.2450.318, Fax: +91.832.2450.602, e-mail: bishwajit@nio.org

Annual subscription price including mail postage is Rs. 2500/= for institutions, companies and libraries and Rs. 2500/= for individuals who are not **ASI** members. The Journal of Acoustical Society of India will be sent to **ASI** members free of any extra charge. Requests for specimen copies and claims for missing issues as well as address changes should be sent to the Editorial Office:

ASI Secretariat, C/o Acoustics and Vibration Metrology, CSIR-National Physical Laboratory, Dr. KS Krishnan Road, New Delhi 110 012, Tel: +91.11.4560.8317, Fax: +91.11.4560.9310, e-mail: asisecretariat.india@gmail.com

ISSN 0973-3302

Printed at Alpha Printers, WZ-35/C, Naraina, Near Ring Road, New Delhi-110028 Tel.: 9810804196. JASI is sent to ASI members free of charge.

ASI

The Journal of Acoustical Society of India

A quarterly publication of the Acoustical Society of India

Volume 52, Number 2, April 2025

ARTICLES

Vibration control in machine structures using constrained multi-layer damping on beams and plates
Alok Kumar Singh, Biswajit Bharat and Amiya Ranjan Mohanty . 42

Multilayer vibration damping coating for mitigation of structural vibrations
Praveen Sreenivasan, Nitin Ahire, Debdatta Ratna and Sangram K. Rath 50

Experimental and numerical investigation of vibration isolator using Transfer Matrix Method (TMM)
P. Rinky Gold, K. Ramji, Padmanabham M. and Udayanand K. 56

Vibration minimization in hydroelectric turbogenerator rotor system using generator support design
Nihar Ranjan Sahoo, Jyothula H. Narayana Rao and J. Srinivas ... 63

Vibration / Noise reduction in multi-rotor drones using optimal phase synchronization method
Bipllab Chakraborty, J.Srinivas and Chikesh Ranjan 71

INFORMATION

Information for Authors Inside back cover

FOREWORD

We are delighted to bring out this special issue of Journal of Acoustical Society of India devoted to the theme 'Vibroacoustics' with emphasis on Vibration Control. Vibroacoustic research focuses on simulation, analysis and control of vibration and noise. As we are all aware, structures play an important role in many engineering applications and vibrations in these structures are to be minimised resulting in minimisation of resultant noise. Hence, Vibration mitigation in structures is widely studied by researchers. Studies on vibration control were driven by advances in damping and isolation approaches Constrained layer and Multi layer damping treatments are being extensively studied as a part of improvising vibration and noise mitigation. Similarly, vibration isolator effectiveness is of prime interest and is being investigated by many researchers in various ways. Another vibration control method under study is flexible rotors, particularly in turbo machinery. Innovative approaches such as phase synchronisation are being attempted in dynamic conditions for robotic applications to minimise vibrations.

This special issue is designed to cover various aspects of vibration control discussed above, through contributed research papers. These include Simulation and experimental study using Constrained and Multilayer damping treatments, Investigation of vibration isolator using Transfer Matrix method, Vibration minimisation using flexible rotor and Phase synchronisation approach for vibration reduction in multi rotor drones. We wish to thank the authors for contributing their papers to this special issue.

PVS Ganesh Kumar
Outstanding Scientist/Scientist H (Retd)

Dr.V Rama Krishna
Scientist 'F'
Naval Science & Technological Laboratory (NSTL)
Defense R&D Organisation (DRDO)
Ministry of Defence, Visakhapatnam - 530 027

The Journal of Acoustical Society of India : Vol. 52, No. 2, 2025 (pp. 42-49)

Vibration control in machine structures using constrained multi-layer damping on beams and plates

Alok Kumar Singh*, Biswajit Bharat and Amiya Ranjan Mohanty
Department of Mechanical Engineering,
Indian Institute of Technology, Kharagpur-721 302, India
e-mail: aloksingh7755@gmail.com

[Received: 05-05-2025; Accepted: 22-08-2025]

ABSTRACT

This study explores the effects of the Constrained Layer Damping (CLD) configurations on the dynamic behavior of beam and plate structures. Utilizing ANSYS finite element based numerical simulations, the influence of single and multiple CLD layers on one and two-dimensional vibrating structures is investigated. The objective of the study is to provide a comprehensive understanding of the impact of these factors on the vibration characteristics and structural integrity of beams and plates. By simulating different CLD conditions, we assess the enhancements of the damping behavior and machine structural stability. In this work the time varying shear modulus of the Viscoelastic Material (VEM) is incorporated within ANSYS using Prony series. This approach leverages frequency dependent loss factor of the material to model its response under dynamic loading conditions. The simulation results offer valuable insights into the effect of optimum CLD layers, highlighting the potential for significant enhancements in vibration isolation. Our findings reveal that the use of multiple constrained layers and multiple material compositions can substantially improve the damping performance. However, the effectiveness of Multi-Layer Constrained Layer Damping (MCLD) can vary based on structural dimensions, the number of layers, and the application conditions. Optimal performance is achieved within a specific range of layers. Detailed analyses of various configurations are presented in this work, which enhances the understanding of damping mechanisms.

1. INTRODUCTION

Metal structures, especially in aerospace and automotive applications, are prone to high vibration amplitudes due to their low inherent damping, which can lead to structural fatigue and noise related failures. To address this, CLD has become a popular choice, leveraging the energy dissipation characteristics of the viscoelastic materials (VEMs) for effective vibration control. Nashif *et al.*[1] brought out that VEMs are particularly effective in damping applications because they store strain energy and dissipate it through hysteresis. David Jones *et al.*[2] elaborated that in CLD, VEM is sandwiched between the base structure and the constraining layer, which forces the VEM to undergo shear deformation during vibrations, thereby dissipating vibrational energy..Sun and Zhang[3] explained that the CLDs are widely used for its ability to enhance vibration control, especially in lightweight and large structures common in the aerospace industry.

In the early 2000s, a significant progress was made in optimizing CLD through both experimental studies and FEA. Pioneering works by Chen and Chan[4] as well as Daya and Potier-Ferry[5], laid the groundwork for understanding the dynamics of CLD in aerospace structures. Subsequent studies by Barbosa and Farage[6] validated these findings experimentally, confirming the accuracy and applicability of FEA models.

Recently, Hujare P. P. *et al.*[7] studied the effects of varying VEM compositions on damping efficiency in sandwich beams. Gröhlich M. *et al.*[8] investigated the temperature-dependent behaviour of VEMs in CLD configurations. The introduction of new materials and composite layers, as investigated by Gröhlich M. *et al.*[9], has further expanded the potential applications of CLD, offering enhanced vibrational control in modern engineering.

Despite extensive research on Constrained Layer Damping, particularly with single-layer applications, there is a significant scope in the exploration of Multiple Constrained Layer Damping configurations. This study addresses this gap by utilizing ANSYS simulations to investigate the dynamic behaviour of beam and plate structures with varying MCLD setups, specifically incorporating the Prony series to model the viscoelastic material.

2. MODELING OF BEAM AND PLATE STRUCTURES

In this section, we detail the modelling of beam and plate structures to investigate the damping effects of various CLD configurations. The materials utilized in the models include Structural Steel for the base structure and the constraining layers, alongside a VEM designated as ZN-1. Aluminium is also used as an alternative material for the constraining layer in each configuration. The specific material properties used are summarized in Table 1.

Table 1. Material and material properties.

Component	Material Name	Density (kg/m³)	Young's Modulus (Pa)	Poisson's Ratio
Base Structure	Structural Steel	7850	2.00×10^{11}	0.3
Viscoelastic Material (VEM)	ZN-1	1010	1.8523 × 10?	0.4
Constraining Layer (CL)	Structural Steel	7850	2.00×10^{11}	0.3
	Aluminium	2770	7.10×10^{1}?	0.33

3. VISCOELASTIC MODELING USING THE PRONY SERIES

Viscoelastic materials exhibit both elastic and viscous behavior, which makes them ideal for damping applications. To accurately model this behavior, the Prony series, a mathematical representation that characterizes the time-dependent stress relaxation modulus of viscoelastic materials is used as demonstrated by Tapia-Romero *et al.*[10]. This section details the process of viscoelastic modeling using the Prony series, which is crucial for our simulations in ANSYS.

3.1 Data Acquisition and Fitting

Using the Dynamic Mechanical Analysis (DMA) machine the storage modulus (G′) and loss modulus (G”) of a material are obtained over a range of frequencies. Subsequently, these values are fitted into a single function denoted as Prony series (see Eqs. (1) and (2)), as mentioned below.

$$G'(\omega) = G_e + \sum_{n=1}^{N} \frac{G_i \omega^2 \tau_i^2}{1 + \omega^2 \tau_i^2} \tag{1}$$

$$G''(\omega) = G_e + \sum_{n=1}^{N} \frac{G_i \omega^2 \tau_i^2}{1 + \omega^2 \tau_i^2} \tag{2}$$

The procedure involves performing DMA tests followed by curve fitting.

Performing DMA Tests: Measure the material's response to sinusoidal stress, capturing G' and G" over the frequencies. In this work the ZN-1 VEM material is used. The storage modulus and shear modulus are obtained from Huang, Z. *et. al.*[11]. The modulus values are shown in Fig. 1 and Table 2.

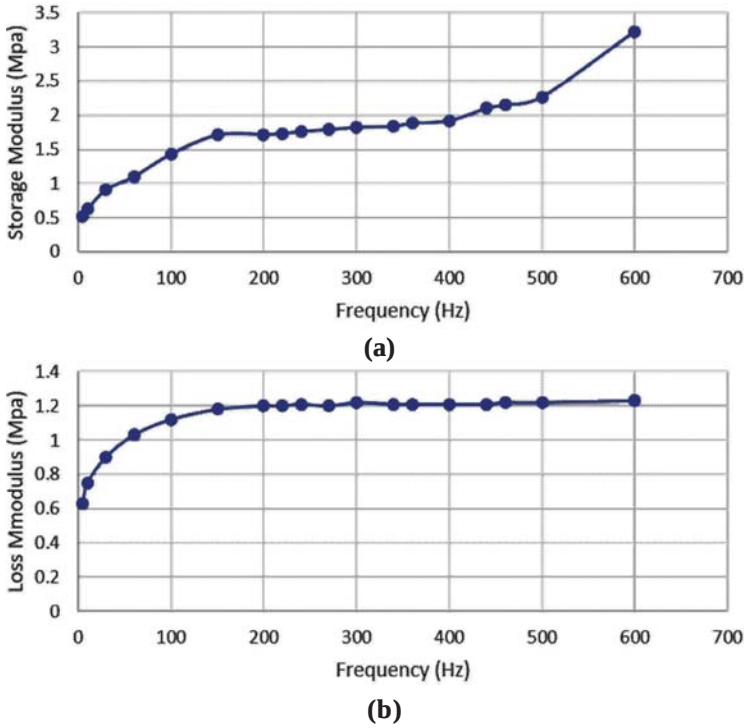

Fig. 1. Shear modulus (a) and loss modulus (b) for ZN-1.

Table 2. VEM Material Data for ZN-1

Frequency (Hz)	Storage Modulus (MPa)	Loss Modulus (MPa)
5	0.51	0.63
10	0.62	0.75
30	0.91	0.9
60	1.1	1.03
100	1.43	1.12
150	1.71	1.18
220	1.73	1.2
240	1.76	1.21
270	1.79	1.2
300	1.82	1.22
340	1.84	1.21
360	1.88	1.21
400	1.92	1.21
440	2.1	1.21
460	2.15	1.22
500	2.27	1.22
600	3.23	1.23

Curve Fitting: Using the equations mentioned in Eqs. (1) and (2), the data is fitted and the values of G_i the Prony coefficients and τ_i the relaxation times. Using these coefficients one can represent the time series for the shear modulus of the VEM material as :

$$G(t) = G_e + \sum_{n=i} G_i e^{-t/\tau i} \tag{3}$$

where, G(t) is the shear modulus at time t, G(∞) is the steady state shear modulus, G_i are the Prony series coefficients, τ_i are the relaxation times. Considering the data mentioned in Table 2, the time series data is evaluated and plotted in Fig. 2.

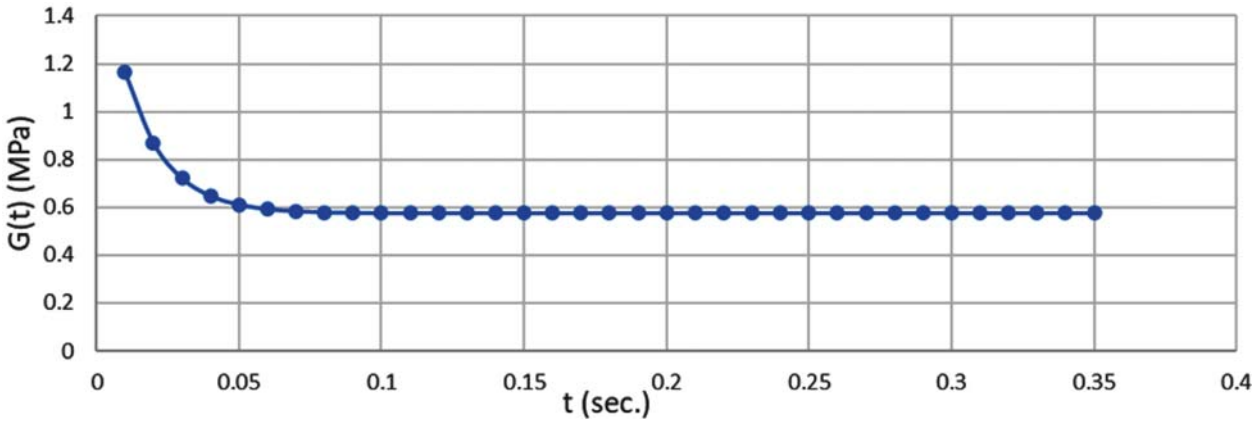

Fig. 2. Relaxation module G(t) in function of time.

4. RESULTS AND DISCUSSIONS

This section presents the results of the modal and harmonic response analyses as described by Mohanty A.R.[12] for the beam and plate structures with various CLD configurations. Identifying the optimal configurations for effective damping the results are discussed.

4.1 Beam Models with CLD Configurations

A beam of length 800 mm, width 100 mm, and height 50 mm is considered. The CL thickness is 2 mm, and the VEM thickness is 5 mm. In this work five different types of configurations of beams with single-layer CLD (S-CLD) and multi-layer CLD (M-CLD) are studied such as: (a) Beam without CLD, (b) Beam with 1 Layer CLD at the top, (c) Beam with 2 Layers of CLD at the top (see Fig. 3), (d) Beam with 1 Layer CLD on both top and bottom surfaces, (e) Beam with 2 Layers of CLD on both top and bottom surfaces.

4.1.1 Modal Analysis of Beam

In the modal analysis of the beam with various CLD configurations, the natural frequencies were found

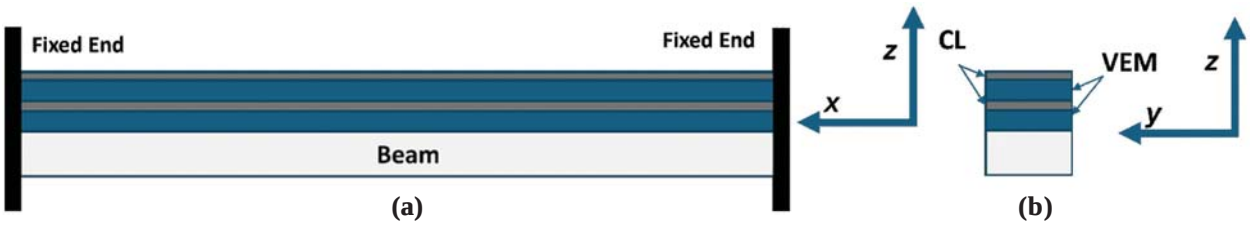

Fig. 3. Beam with 2-layer CLD on Top (a) front view, (b) cross-sectional view.

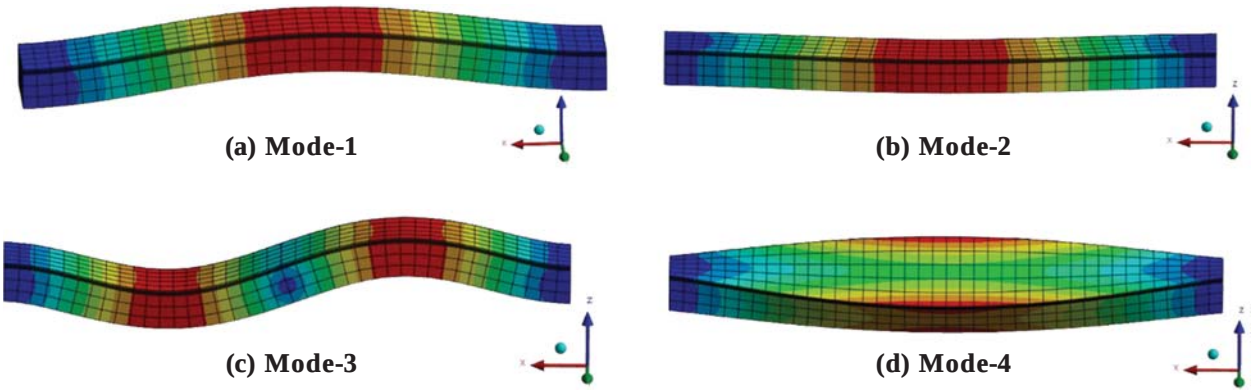

Fig. 4. Mode shapes of a Clamped-Clamped Beam with single layer CLD. (a) Mode-1 corresponds to the modal vibration along (transverse) z-axis, (b) Mode-2 corresponds to the modal vibration along (transverse) y-axis (c) Mode-3 corresponds to the modal vibration along (transverse) z-axis (d) Mode-4 corresponds to the angular vibration about the x-axis

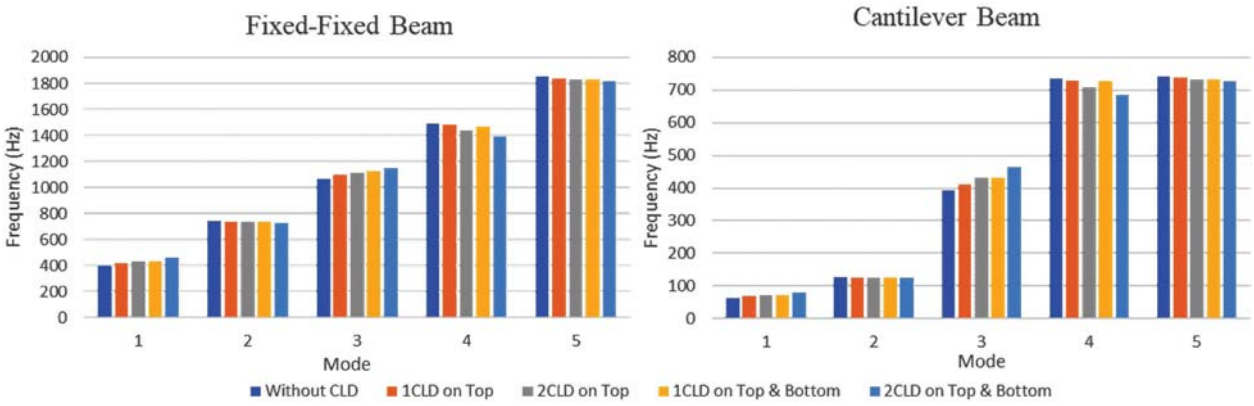

(a) **(b)**

Fig. 5. Natural Frequencies of (a) Fixed-Fixed Beam and (b) Cantilever Beam with steel as CL.

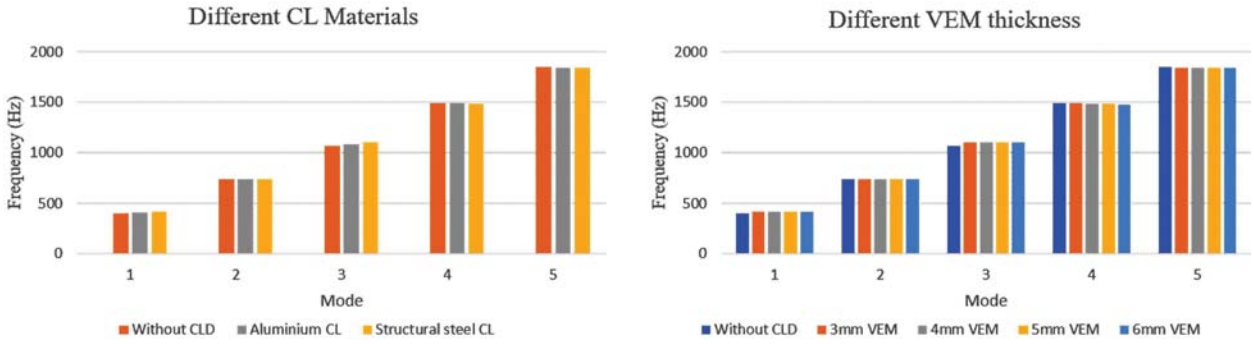

(a) **(b)**

Fig. 6. Natural Frequencies of Fixed-Fixed Beam for (a) different CL materials and (b) different VEM thickness for steel as CL (2 mm thickness).

to be influenced by the alignment of the modes with the direction of the applied CL. Specifically, the 1st and 3rd modes, are influenced by the presence of the CL layers. As the CL layers are applied on the top

part of the x-y plane of the beam (see Fig. 3), the modal vibrations along the perpendicular plane (i.e., along z-axis), shows an increase in natural frequencies due to enhanced stiffness. Conversely, modes not aligned with the CLD application experienced a decrease in natural frequencies due to the added mass. This highlights the significance of strategic CL placement in optimizing the dynamic behaviour of structures. It has also been observed that the effect of aluminium as CL is smaller than the steel CL.

4.1.2 Harmonic Response of Beam

It has been observed from Fig. 7 that the Structural steel performs better than the aluminium as a constraining layer, due to its higher stiffness. Additionally, by changing the VEM thickness in 1CLD configuration the 5mm thickness VEM performs better than the other configurations (see Fig. 8). The harmonic response analysis highlights the critical role of Constrained Layer Damping (CLD) configurations in optimizing vibration control in beam structures. For fixed-fixed beams, applying CLD on both the top and bottom surfaces provided superior vibration isolation (see Fig. 9), demonstrating the importance of strategic CLD placement. In cantilever beams, a single layer CLD performs better (see Fig. 10). These findings underscore the necessity of precise CLD application, material choice, and VEM thickness for effective vibration mitigation in engineering structures for different boundary constraints.

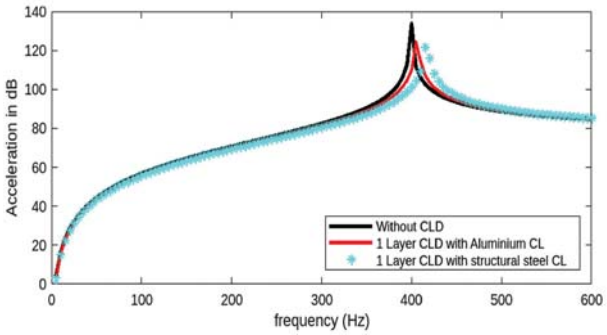

Fig. 7. Frequency Responses of diff. CL Material.

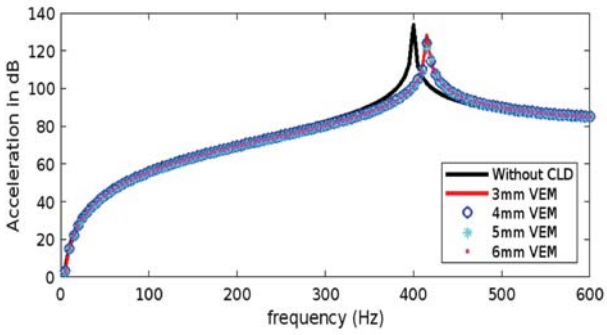

Fig. 8. Frequency Responses of diff. VEM thickness.

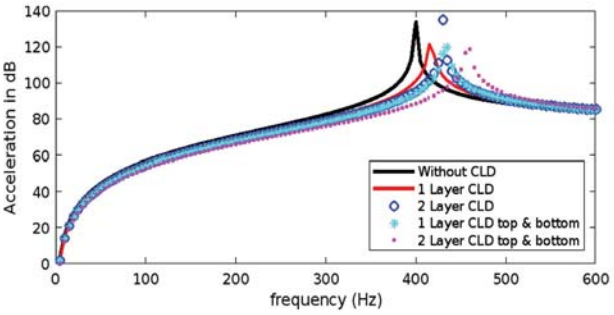

Fig. 9. Frequency Responses of Fixed-Fixed Beam.

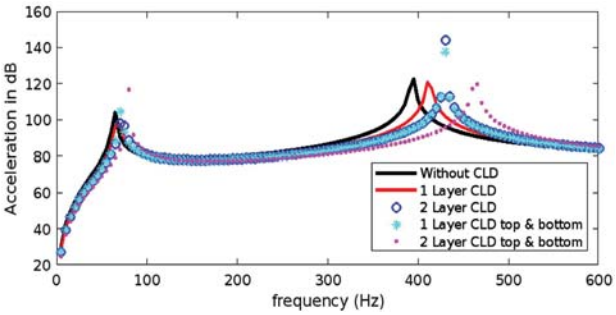

Fig. 10. Frequency Responses of Cantilever Beam.

4.2 Plate Models with CLD Configurations

In this case, a plate with length 600 mm, width 400 mm, and thickness 10 mm is studied. The CL thickness is set at 2 mm, and the VEM thickness is 5 mm. Four different types of configurations of beams with SCLD or MCLD are studied such as: (a) Plate without CLD, (b) Plate with 1 Layer CLD at the top, (c) Plate with 2 Layer CLD at the top, (d) Plate with 1 Layer CLD on both top and bottom surfaces.

4.2.1 Modal Analysis (Plate)

The modal analysis of the plate structures demonstrates that the natural frequencies increase with the addition of more CLD layers. This increase indicates enhanced stiffness in the plate, due to addition of constrained layers. Each additional layer adds rigidity to the plate, raising its natural frequencies and reducing vibration amplitudes. This effect of CLD not only controls vibrations but also allows for tuning the structure's dynamic properties to avoid resonance, improving overall structural performance.

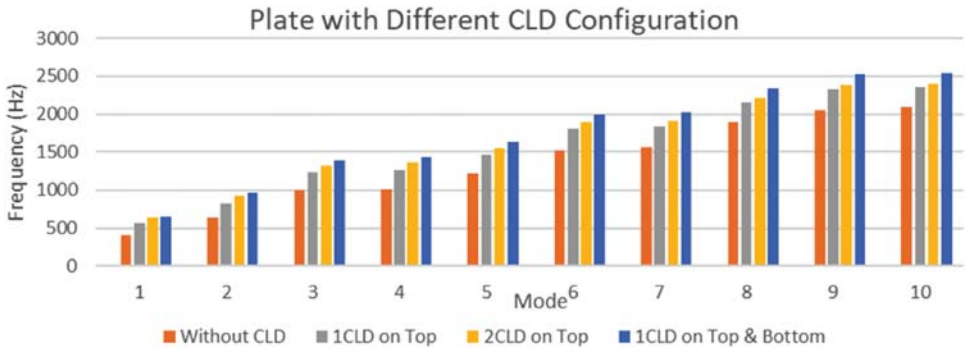

Fig. 11. Natural Frequency of Plate with Fixed at four edges.

4.2.2 Harmonic Response Analysis (Plate)

The harmonic response analysis for the plate structure reveals a consistent improvement in vibration isolation as the CLD configurations are enhanced. With each incremental upgrade in the CLD setup, the damping effectiveness increases, leading to better control over vibrational energy. This trend underscores the effectiveness of CLD in reducing vibrations, particularly when the configurations are optimized. The results highlight that strategically designed CLD layers significantly enhance the vibration isolation capabilities of plate structures, making them more resilient to dynamic loading conditions.

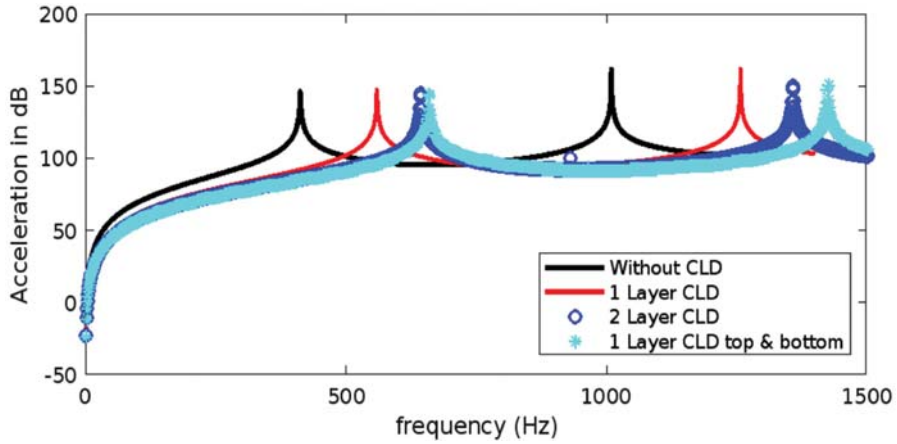

Fig. 12. Frequency Responses of Plate.

5. CONCLUSION

This research thoroughly examined the impact of Constrained Layer Damping (CLD) configurations on the vibrational behaviour of beams and plate structures. The findings provide significant insights for

optimizing vibration control in engineering applications. Notable conclusions highlight the criticality of strategic CLD placement, material selection, and layer thickness optimization. The optimal parameters were found to be contingent on the boundary constraints of the structures. For a Fixed-Fixed beam, a configuration with a 5mm thick Viscoelastic Material (VEM) layer and 2 mm CL on both the top and bottom is suitable. In contrast, for a cantilever beam, a single layer on top is more effective due to the presence of a free end. For a plate fixed at all four edges, a configuration with one layer on both the top and bottom, using 5mm VEM and 2mm Constrained Layer (CL), is more efficient. Additionally, steel was found to be a superior choice for the constrained layer over aluminium in all scenarios.

REFERENCES

[1] A.D. Nashif, D.I.G. Jones and J.P. Henderson, 1991. *Vibration Damping*, John Wiley & Sons.

[2] David I.G. Jones, 2001. *Handbook of Viscoelastic Vibration Damping,* John Wiley & Sons.

[3] C.T. Sun and X.D. Zhang, 1995. Use of thickness-shear mode in adaptive sandwich structures, *Smart Mater. Struct.*, **4**(3), 202.

[4] Q. Chen and Y.W. Chan, 2000. Integral finite element method for dynamical analysis of elastic-viscoelastic composite structures, *Comput. Struct.,* **74,** 51-64.

[5] E.M. Daya and M. Potier-Ferry, 2002. A shell finite element for viscoelastically damped sandwich structures, *Rev. Eur. Élém.*, **11,** 39-56.

[6] F.S. Barbosa and M. Farage, 2008. A finite element model for sandwich viscoelastic beams: Experimental and numerical assessment, *J. Sound Vib.,* **317,** 91-111.

[7] P.P. Hujare and A.D. Sahasrabudhe, 2014. Experimental investigation of damping performance of viscoelastic material using constrained layer damping treatment, *Procedia Mater. Sci.,* **6,** 1322-1328.

[8] M. Gröhlich, A. Lang, M. Böswald and J. Meier, 2021. Viscoelastic damping design - Thermal impact on a constrained layer damping treatment, *Mater. Des.,* **207,** 109885.

[9] M. Gröhlich, M. Böswald, and J. Wallaschek, 2023. Viscoelastic damping design - A novel approach for shape optimization of constrained layer damping treatments at different ambient temperatures, *J. Sound Vib.,* **555,** 117703.

[10] M.A. Tapia-Romero, M. Dehonor-Gómez and L.E. Lugo-Uribe, 2020. Prony series calculation for viscoelastic behavior modeling of structural adhesives from DMA data, *Ing. Investig. Tecnol.*, **21**(2), e1668.

[11] Z. Huang, X. Wang, F. Chu, J. Wu and J. Luo, 2019. A finite element model for the vibration analysis of sandwich beam with frequency-dependent viscoelastic material core, *Materials,* **12**(20), 3390.

[12] A.R. Mohanty, 2014. Machinery Condition Monitoring: *Principles and Practices,* CRC Press, Boca Raton, FL, USA.

The Journal of Acoustical Society of India : Vol. 52, No. 2, 2025 (pp. 50-55)

Multilayer vibration damping coating for mitigation of structural vibrations

Praveen Sreenivasan*, Nitin Ahire, Debdatta Ratna and Sangram K. Rath
Naval Materials Research Laboratory, Shil-Badlapur Road,
Anand Nagar PO, Ambernath-421 506, India
e-mail: praveens.nmrl@gov.in

[Received: 10-08-2025; Accepted: 22-08-2025]

ABSTRACT

Passive vibration damping using polymer based viscoelastic materials is a well-established approach for mitigating the structural vibrations. However, it is an ongoing challenge to damp structural vibrations in a wide frequency range. In the present paper, a multilayer constrained layer damping (MCLD) approach is reported with efficacious vibration damping in a wide frequency range of 100-1000 Hz. To this end, carbon black reinforced nitrile butadiene rubber-polyvinyl chloride (NVC) elastomeric blend and polyether diamine cured epoxy resin were used as viscoelastic materials (VEMs). The VEMs were characterized for their viscoelastic properties as a function of temperature by dynamic mechanical analysis (DMA). Thereafter, the VEMs were employed to construct five layer MCLD coatings and evaluated for their system loss factors by using an electrodynamic shaker. The effect of VEM type, positioning of the VEM, role of interfacial adhesive layer on the vibration damping efficacy of the MCLD systems were investigated. The results revealed that higher loss factors for the elastomers blends did not translate into corresponding system loss factors in the MCLD configuration. However, using an epoxy based VEM resulted in a significantly higher system loss factor (0.15 to 0.24) in the frequency range of 100-2000 Hz.

1. INTRODUCTION

Reducing structural vibrations is crucial for maintaining the strategic advantage of naval fleet, as the noise emitted underwater can be detected by potential adversaries. In order to address structural vibration problem, various mitigation strategies are employed. There are two primary approaches for structural vibration damping: passive and active methods[1-4]. Active damping methods involve the use of electronic instruments, such as actuators and sensors, to actively control and reduce vibrations in mechanical systems[5,6]. These methods require external power and control systems to monitor the vibrations and apply appropriate forces to counteract them[7]. Passive damping, on the other hand, refers to the use of materials that dissipate vibration energy without the need for external power or control systems[8]. The efficacy of passive vibration damping spans a broad frequency range, making it versatile in addressing various vibration sources.

In passive damping techniques, viscoelastic materials (VEM) can be utilized in two ways: free layer damping (FLD) and constrained layer damping (CLD)[1]. Among the plethora of materials reported for

use in CLD in the literature, elastomers are considered to be effective VEMs for CLD, owing to their flexibility, tunability of loss factor and ease of application[9]. However, most of the studies on VEMs reported in literature pertain to their evaluation of loss factor from DMA[10]. Reports on their analysis at system level (CLD or FLD) representing the real time scenario of their application is rather scanty[11]. Further, literature reports on vibration damping through CLD approach are primarily focused on three layer configurations with scanty reports on multilayer configurations[1-4]. In view of the above, the objective of the present study is to investigate the vibration damping efficacy of multilayer vibration damping coatings (MCLD) in a five layer constrained layer configuration. This system facilitates use of two layers of VEMs having complimentary viscoelastic properties.

2. EXPERIMENTAL DETAILS

2.1 Materials

NVC blend with 70% NBR (acrylonitrile content = 33%) and 30% PVC by weight, with a Mooney viscosity (ML 1+4 @100°C, MU) of 60 ± 5 and density of 1.11 ± 0.02 g/cc and the reinforcing filler carbon black (Grade N220) with a BET surface area of 114 ± 5 m^2/g and mean oil absorption value of 114±6 ml/100 g were the materials used for this study. A sulphur based vulcanization system was used for curing of the rubber compound. Rubber processing grade dioctyl phthalate (DOP) was used as a plasticizer. DGEBA (diglycidyl ether of bisphenol A, Araldite LY 556) was the epoxy resin (epoxy equivalent = 195 ± 5 g/equivalents) used for preparation of the thermoset based VEM. Polyether diamine was used as the curative for the epoxy resin.

2.1.1 Preparation of carbon black reinforced NVC blend

The NVC blends with varied contents of carbon black (0-40phr) and other ingredients were compounded using a laboratory two roll mill set up. The rubber compounds were subsequently vulcanized at their respective t90 using a hot press at 150°C and a pressure of 5 MPa. The NVC vulcanizates were nomenclatured according to their carbon black content i.e., NVC CB10, NVC CB20 and NVC CB40 while the pristine blend has been referred to as NVC.

2.1.2 Preparation of polyether diamine cured epoxy thermoset

Epoxy resin based VEM was prepared by curing of epoxy resin using stoichiometric amount of polyether diamine. The epoxy and diamine mixture was homogenized using a mechanical stirrer. The homogenized mixture was then cast on a Teflon mould for curing at ambient temperature for 12 h. The epoxy resins cured with polyether diamines have been referred EP-LM.

2.2 Characterization methods

2.2.1 Dynamic mechanical analysis

Measurements of frequency and temperature dependent viscoelastic properties[12] were conducted on the materials utilizing an RSA G2 TA dynamic mechanical analyser (DMA). The temperature sweep was executed in a single cantilever mode with a programmed heating rate of 5 °C/min, frequency of 1 Hz at a strain of 0.05% within the range of -30°C to 140 °C.

2.2.2 Construction of five layer CLDs

Three CLD systems with five layer configurations were constructed using the elastomeric NVC blend and epoxy thermosets as VEMs. The constituting elements of the five layer MCLD systems were (a) 12 mm thick Mild Steel (MS) as the substrate and alternate layers of VEM and MS constraining layer (CL). Three VEM combinations were studied. (1) NVC-NVC system (2) NVC-Epoxy system and (3) Epoxy-Epoxy system. The generic process for construction of the CLD systems is as follows: In order to construct CLD system (a), the surface of the MS beam was slightly roughened with a sand paper (grit size 100) and then degreased with ethyl acetate and then allowed to dry. The surface of the NVC elastomers sheets were

slightly abraded with a sand paper (grit size 200) and degreased with acetone. In order to investigate the effect of adhesive type on vibration damping efficacy of CLD system, three different types of adhesives were used to adhere the elastomeric sheets onto substrate and CL layers. The different adhesives used were: (a) solvent and chlorinated rubber based one component adhesive (b) two component epoxy based solvent free adhesive and (c) two component rubber toughened epoxy based adhesive with a solvent content of 70 wt. %. The adhesives were applied in both the surface treated elastomeric sheets and MS beam and then joined together by gentle pressing. The adhesives were used only when elastomer material is used as VEM. In the case of epoxy based VEM, the VEM itself acted as adhesive layer.

2.2.3 Vibration damping measurements

The vibration damping measurements of the bare MS beam and the five layer CLD systems were carried out using an electrodynamic shaker (DS-1000 system with 1000 kgf capacity). In this test set up, one end of the test specimens was clamped and the other end was excited with a sweeping rate of one octave per minute having a frequency resolution of 0.67 Hz. Accelerometers (sensitivity of 100 ± 3 mV/g) were used to record sample acceleration. An 8 channel data acquisition system was used to obtain the time-dependent response which was then transformed into the frequency domain using Fast Fourier transform (FFT) to generate the frequency response function (FRF). The circle-fit modal analysis technique was then employed to identify the natural frequencies, loss factor, and mode shapes of the CLD specimens[13].

3. RESULTS AND DISCUSSION

3.1 Dynamic mechanical analysis of VEMs

It is well established that the viscoelastic properties of polymers play a critical role in their efficacy for vibration damping[1]. In the present study, two different types of VEMs have been used for vibration damping studies in a multilayer CLD configuration; (a) carbon black reinforced NVC blend and (b) polyether diamine cured epoxy thermoset.

3.1.1 Carbon black reinforced NVC blend

Fig. 1 shows the viscoelastic properties of the pristine NVC matrix as well as the carbon black reinforced vulcanizates, as a function of temperature at fixed frequency of 1Hz.

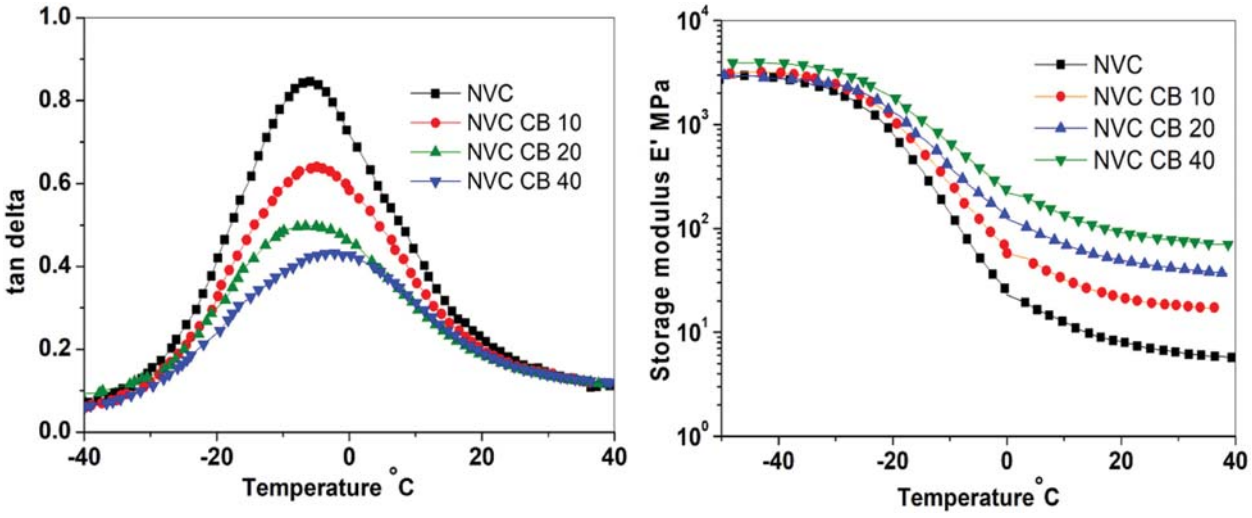

Fig. 1. DMA of NVC blends (a) tan δ vs. *T* (b) storage modulus (E') vs. *T*.

First, focusing on the dissipation or loss factor (tan δ) vs. T profiles shown in Fig. 1(a), it is observed that the pristine NVC is characterized by a single tan δ peak, located at –6°C corresponding to α relaxation temperature. The observation of a single tan δ peak for the NVC blend implies miscibility of NBR and PVC at this composition. Incorporation of carbon black leads to reduction in the tan δ peak height with no discernible change in the peak position. A significant drop in the peak intensity is observed at 40 phr loading of carbon black with a broadening of its profile towards the high temperature region. From the storage modulus, *E'* vs. *T* profiles, shown in Fig. 1(b), carbon black induced reinforcement of the NVC matrix is evident in both the glassy and rubbery regions.Usually a tan δ peak intensity of $\geq$ 0.30 over a broad temperature range is considered as a benchmark figure for effective vibration damping[14]. Based on this criterion the carbon black reinforced PVC-NBR elastomers can be considered as candidature materials for MCLD applications, despite the carbon black induced decrease in tan δ peak intensities.

3.1.2 Polyether diamine cured epoxy

Fig. 2 illustrates the temperature dependent viscoelastic properties of the epoxy based material (EP-LM). Fig. 2(a) and 2(b) show the material loss factor (tan δ) vs. temperature and storage modulus vs. temperature profiles of the two systems. The EP-LM system, exhibits a tan δ peak at 21°C with a significantly higher peak intensity value of 1.06. These results can be reconciled with the lower cross-link density of EP-LM system. Further, the tan δ profile for EP-LM system is significantly broader (full width at half maximum of 29.8°C). Owing to the higher tan δ intensity of EP-LM system, it can be considered as a more effective VEM across broad frequency range. Fig.2(b) shows the storage modulus vs. T profile EP-LM thermoset. The results indicate the material is compliant in the temperature region of interest for effective damping. From these results it can be inferred that EP-LM system is a candidate VEM for MCLD applications.

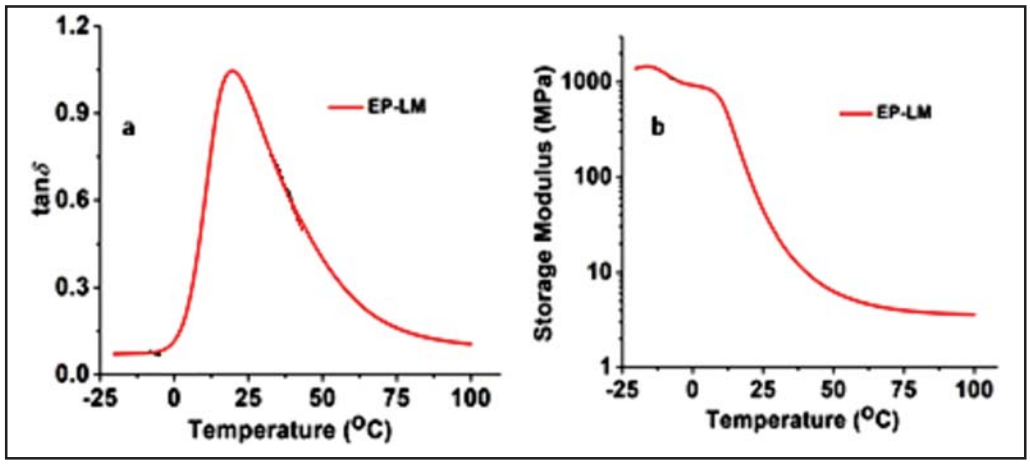

Fig. 2. Dynamic mechanical analysis results of EP-LM system (a) tan δ vs. temperature profile (b) storage modulus vs. temperature profile.

3.2 Vibration damping measurements

The bare beam and MCLDs were excited using an electrodynamic shaker. The MCLD system loss factor (SLF) was determined at each modal frequency using the modal circle fit method and the results are shown in Fig. 3. Fig. 3(a) shows the system loss factor of the five layer CLD system with two layers of NVC as the VEM layers constructed with three different types of adhesives. From the results it is observed that this MCLD system shows higher system loss factor values in the low frequency region and then monotonically decreases with increasing frequency. Further, the system loss factor value is influenced by the type of adhesive used to construct the MCLDs. In case of MCLD system constructed with alternative layers of NVC and EP-LM as VEMs (Fig. 3(b)), a similar trend of higher system loss factor at lower

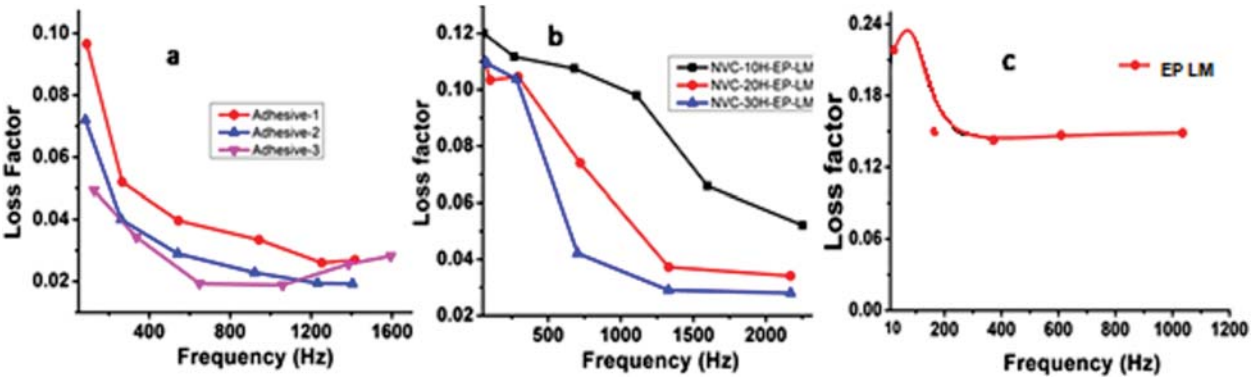

Fig. 3. MCLD system loss factor as a function of frequency (a) System of two layers of NVC as VEM constructed with three different adhesives (b) NVC and EP-LM based MCLD system with varied carbon black in NVC matrix (c) EP-LM VEM based MCLD system.

frequencies (0.10 to 0.12 < 200 Hz) followed by a monotonic decrease at higher frequency modes of vibration is noticed. Fig. 3(c) shows the frequency dependence of system loss factor for the MCLD system constructed with two layers of EP-LM as the VEM. From the results, it is seen that the system loss factor values for this system are significantly higher compared to the other two MCLD systems at all modal frequencies. Further, in this system the loss factor values do not register the decreasing trend noticed for the NVC and NVC-EP-LM based MCLD system with increased frequency.

Thus the comparative modal analysis of the three different MCLD configurations reveals that epoxy based VEMs show superior vibration damping performance compared to other VEM combination studied. A plausible reason for the said observation is the absence of interfacial adhesive layer in case of epoxy based VEMs, which seems to have a detrimental effect in vibration damping efficacy of elastomers based MCLD systems.

4. CONCLUSION

In summary, the study focused on four main aspects: (a) the development of carbon black reinforced NBR-PVC blend and epoxy thermoset-based VEMs, (b) the evaluation of their temperature-dependent viscoelastic properties using DMA, (c) construction of five-layer MCLD systems using the developed VEMs and metal substrate (MS) as the constraining layer, and (d) the modal analysis of the MCLDs utilizing an electrodynamic shaker. Key findings of the study indicate that the system loss factor values for MCLDs with two layers of elastomeric blend were sensitive to the type of the adhesive layer used in construction. Similar observations were noted for five-layer MCLDs constructed with alternating layers of elastomer blend and epoxy thermoset as VEMs. In contrast, the use of two layers of epoxy-based VEM, obviating the need for an external adhesive, consistently demonstrated higher loss factor values in the frequency range of 100-1000 Hz. The study suggests that this multilayer CLD approach with epoxy based VEMs holds potential for mitigating structural vibrations in the engine room foundation and machinery base frames of surface ships.

REFERENCES

[1]. X.Q. Zhou, D.Y.Yu, X.Y. Shao, S.Q. Zhang and S. Wang, 2016. *Comp. Structures,* **136,** 460.

[2] D.D.L. Chung, 2001. *J. Mater. Sci.,* **36,** 5733.

[3] Z. Li and M.J. Crocker, 2005. *Int. J. Acoust. Vib.,* **10,** 159.

[4] Muhammad B.B., Wan M., Feng J. and Zhang W. H., 2017. *Int. J. Adv. Manuf. Technol.* **89,** 2935.

[5] Z. Huang, F. Huang, X. Wang and F. Chu, 2022. *Materials,* **16,** 95.

[6] A. Masa'id, B.W. Lenggana, U. Ubaidillah, D.D. Susilo and S.B. Choi, 2023. *Actuators,* **12,** 113.

[7] A.M. Baz, 2019. *Active and passive vibration damping*. John Wiley & Sons.

[8] B.C. Chakraborty and D. Ratna, 2020. Polymers for vibration damping applications. *Elsevier*.

[9] Y. Hou, Y. Peng, P. Li, Q. Wu, J. Zhang, W. Li and W. Wu, 2022. *J. ACS Appl. Mater.* Interface, **14,** 35097.

[10] M. Masoomi, A.A. Katbab and H. Nazockdast, 2006. *Polym. Compos,* **27,** 461.

[11] M. Anthamatten, S.W. O'Neill, D. Liu,T.M. Wheler, R.S.Vallery, D.W. Gidley, 2018. *Macromolecules,* **51,** 2564-2571.

[12] J.D. Ferry, 1980. *Viscoelastic properties of polymers.* John Wiley & Sons.

[13] K.B. Elliott and L.D. Mitchell, 1984. The improved frequency response function and its effect on modal circle fits. *J. Appl. Mech.,* **51**(3): 657-663

[14] J. James, G.V. Thomas, K.P. Pramoda, N. Kalarikkal and S. Thomas, 2018. *New J. Chem.,* **42,** 1939.

The Journal of Acoustical Society of India : Vol. 52, No. 2, 2025 (pp. 56-62)

Experimental and numerical investigation of vibration isolator using Transfer Matrix Method (TMM)

P. Rinky Gold[1*], K. Ramji[1], Padmanabham M.[2] and Udayanand K.[2]

[1]Department of Mechanical Engineering, College of Engineering, Andhra University, Visakhapatnam -530 003, India

[2]Naval Science and Technological Laboratory, DRDO, Visakhapatnam-532 007, India

e-mail: rinkygold7@gmail.com

[Received: 04-08-2025; Accepted: 22-08-2025]

ABSTRACT

Unwanted vibrations from engines, motors, and other movable components can affect performance and cause undesired outcomes. Effective vibration isolation is essential, and insertion loss is a key metric to evaluate its effectiveness. This study investigates spring mounts using the Transfer Matrix Method (TMM) to find insertion loss through both experimental and numerical approaches. A test specimen with six identical spring isolators between an upper and lower plate, weighing 195 kg, was used for experimentation. Transient data from impact hammer tests was used for validation through ANSYS simulations and modal analysis confirmed the natural frequencies of the system. Harmonic analysis further determined the insertion loss using TMM derived from the mobility matrix. These results provide valuable insights for designing more effective isolators in various industries.

1. INTRODUCTION

The most reliable way of reducing the vibrations caused by machines or any other moving components is by isolating the vibrating source from its immediate surroundings (that are usually connected to the source). Vibration isolation aims to minimize the vibration level at a designated receiver by introducing an impedance change along the vibration path. This is typically achieved using a compliant element, such as a spring or rubber isolator. While isolation is generally effective across a broad frequency range, it is well established that structural modes of isolators, often referred to as surge frequencies, allow energy to propagate efficiently. With increasing demand for quieter products, structure-borne energy transmission through isolators has become a significant concern.

The performance of a vibration isolator is influenced by its dynamic characteristics and those of the system it interacts with. In many cases, the isolator's mass is overlooked, and it is modeled solely as a frequency-dependent spring. Isolators are often modeled as a linear component termed a dynamic stiffness (kd) defined as[1].

$$k_d = \frac{j\omega F}{v_1 - v_2} \tag{1}$$

Where, v_1, v_2, and F represent the velocities at the inlet and outlet sides of the mount, respectively, and the dynamic force. Note that this definition of dynamic stiffness assumes that the force is equivalent on both sides of the isolator, neglecting the inertia effects of the isolator.

Although it remains a linear method, the transfer matrix approach offers a more comprehensive representation of an isolator by accounting for inertial effects. The force and velocity on one side of the isolator F1 and v1 are connected to those on the opposite side F_2 and v_2 through four-pole parameters (a_{11}, a_{12}, a_{21}, a_{22}). This relationship can be written as[1].

$$\begin{bmatrix} F_1 \\ v_1 \end{bmatrix} = \begin{bmatrix} a_{11} & a_{12} \\ a_{21} & a_{22} \end{bmatrix} \begin{bmatrix} F_2 \\ v_2 \end{bmatrix} \tag{2}$$

The four-pole parameters are frequency-dependent and complex. Fig.1 presents a schematic of an isolator, indicating the forces (F_1 and F_2) and velocities (v_1 and v_2), along with the defined direction convention.

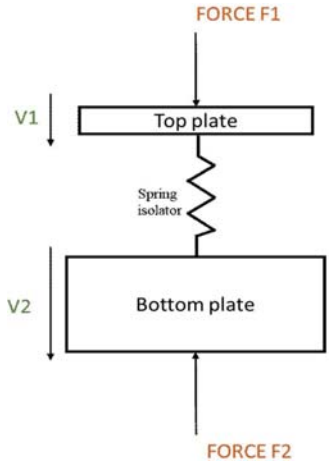

Fig. 1. Schematic illustrating mount with force and velocity variables.

It is acknowledged that Molloy[1] was the first to suggest using four-pole metrics to assess isolator features. Eventually, Snowdon[2] developed four-pole parameters for a variety of reduced mechanical models, building upon this idea and applying it to vibration isolation. This idea strongly resembles that of Munjal[3], who used a comparable methodology while studying acoustic waveguides, including mufflers. Dickens and Norwood[4] and Dickens[5] then came up with an experimental procedure that used two masses to find an isolator's four-pole characteristics. This method is flexible enough to be used with both symmetric and asymmetric isolators because measurements were made twice with differing floating masses on the receiver side.

Kim and Singh's[6,7] research concentrated on elastomeric isolators by employing a more sophisticated mobility matrix technique. They compared analytical and experimental results using a multi-axial model for isolators. The transfer matrix approach, which has the benefit of using more representative measures for assessing isolator performance, is highlighted in the current work. We applied the same idea to a multiple isolator system after Sun Shishuo[8] applied the TMM to a single helical spring isolator. Transmissibility, or the ratio of the magnitudes at the input and output sides of an isolator, is one commonly used statistic, either displacement or force can be used to define this. Transmissibility depends on the properties of both the source and the receiver in addition to the isolator, while being easy to measure and offering helpful information. On the other hand, while pre-loads may have an impact, the transfer matrix of an isolator is mostly determined by the isolator itself. It was suggested by Ungar[9] to use isolator effectiveness (E), which is equivalent to insertion loss as brought out by Izak[10]. This metric's main benefit is that it includes the compliance of the source and recipient structures in the assessment. As seen in Fig.

2, isolator insertion loss quantifies the decibel difference between the isolated and unisolated responses. It can be represented mathematically as[1].

$$1L = 20Log_{10} = |\mathrm{E}| = 20Log_{10} \frac{|v_f rigid|}{|v_f isolated|} \tag{3}$$

Where v_f rigid and vf isolated are the unisolated and isolated vibrations respectively. It can be expressed in terms of the four pole parameters as[1]

$$1L = 20Log_{10} \left| a_{11} + \frac{a_{12} Y_1 Y_2}{Y_1 + Y_2} + \frac{a_{21}}{Y_1 + Y_2} \right| \tag{4}$$

Where Z_S and Z_R are the mechanical impedances on the source and receiver side respectively.

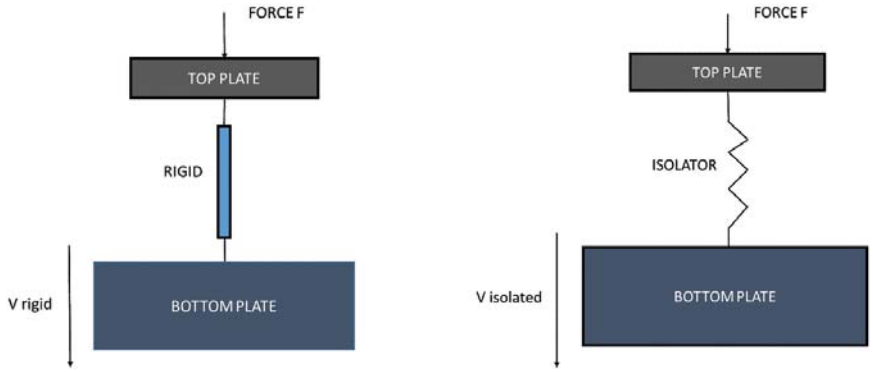

Fig. 2. Schematic illustrating isolator insertion loss, with Rigid and isolator connections.

This paper suggests two related approaches to use finite element analysis to find the transfer matrix of an isolator. To take into consideration the stress-stiffening effects brought on by the static preload, a static analysis must be done first. The context for the ensuing dynamic analysis is established by this static study. After that, a modal analysis is carried out, accounting for the preload, to determine the structural modes. To find the transfer matrix, first get the mobility matrix from two consecutive forced response analyses with various loading scenarios. It has been demonstrated that this method produces consistent findings for insertion loss.

The described methodology was applied to a test specimen modelled in ANSYS, and insertion loss was determined through harmonic analysis. The model's accuracy was validated by comparing the natural frequencies obtained from experimental data with those from modal analysis along with the response collected using an impact hammer during experimentation.

2. DETERMINATION OF TRANSFER MATRIX METHOD (TMM)

Initially, a static finite element analysis is performed to account for the static preload, which can be either linear or nonlinear. This analysis aims to update the stiffness matrix to incorporate the effects of stress stiffening caused by the preload. If the preload does not substantially affect the structural modes of the isolator, then the static analysis may be deemed unnecessary. The steps involved in obtaining the TMM are as follows :

Step 1 : Static analysis carried out with a preload of 2500N.

Step 2 : Modal analysis with the preload and without the preload.

Step 3 : Forced response analyses were done twice to capture the velocities in the frequency domain.

2.1 Mobility matrix technique

The TMM is being formed using the mobility matrix technique. First, the mobility matrix is formed by conducting harmonic analysis using two different boundary conditions for the first and second analyses, which are as follows[1] :

$$F_1 = 1 \text{ and } F_2 = 0 \tag{5}$$

$$F_1 = 0 \text{ and } F_2 = 1 \tag{6}$$

The mobility matrix is as follows,

$$\begin{bmatrix} v_1 \\ v_2 \end{bmatrix} = \begin{bmatrix} b_{11} & b_{12} \\ b_{21} & b_{22} \end{bmatrix} \begin{bmatrix} F_1 \\ F_2 \end{bmatrix} \tag{7}$$

Here, b_{11}, b_{12}, b_{21} and b_{22} will be the mobility matrix terms. And these are obtained using Equations (5), (6)

$$b_{11} = \frac{v_1}{F_1} \text{ and } b_{21} = \frac{v_2}{F_1} \tag{8}$$

$$b_{12} = \frac{v_1}{F_2} \text{ and } b_{22} = \frac{v_2}{F_2} \tag{9}$$

Where, v_1, v_2, F_1 and F_2 are determined from analyses with the respective boundary conditions indicated. Now the TMM terms or the Four Pole parameters are obtained as :

$$a_{11} = -\frac{b_{22}}{b_{21}}, a_{12} = \frac{1}{b_{21}}, a_{21} = b_{12} - \frac{b_{11}b_{22}}{b_{21}} \text{ and } a_{22} = \frac{b_{22}}{b_{21}} \tag{10}$$

All the terms of mobility and the transfer matrix are frequency-dependent.

3. EXPERIMENTAL PROCEDURES

The numerical analysis was performed using ANSYS, and a comprehensive experimental investigation was carried out to validate the findings and assess the performance of the vibration isolator. This section deals with the experimental setup, procedures, and measurements employed to gather data during experimentation on the test specimen for comparison with the numerical results. Specifically, acceleration response in the time domain was collected from both the top and bottom of the test specimen. This data forms the basis for further analysis and comparison with the ANSYS. Fig. 3 shows the test specimen with the top plate and bottom plate (connected to a bottom raft) in between six helical springs that have been placed symmetrically. Fig. 4 shows the devices and instruments used for the experimentation.

Fig. 3. Shows the helical spring isolator and the test specimen.

Fig. 4. Shows the DAQ, impact hammer, and sensor type used.

The Data Acquisition System (DAQ) used was DewesoftX SIRIUS 16-channel. A B & K impact hammer with 0.225 mV / N sensitivity and a maximum force of 35,584 N was utilized. Two DYTRAN 3055B2 sensors with 10 mV / g sensitivity were used to measure vibrations on the top and bottom plates by impacting the top plate. The spring isolator dimensions were, wire diameter (d) of 8 mm, spring diameter (D) of 63 mm, height of the spring was 94 mm and pitch of the spring was 15 mm with active turns (n) of 5 and total number of turns are 7, where G is the shear modulus of value 76.9 GPa.

Now the spring stiffness can be determined from[8]

$$k = \frac{Gd^4}{8nD^3} \tag{11}$$

The static stiffness determined using the above-mentioned formula was 31,500 N / m, comparing this value with the stiffness value obtained from ANSYS, they coincided well. Now the acceleration data in the time domain was extracted by conducting the experimentation for 10 seconds where this time domain data was converted to frequency through Fast Fourier Transforms (FFT) to understand the natural frequencies from experimentation.

4. COMPARISON OF RESULTS BETWEEN EXPERIMENTATION AND ANSYS

As mentioned earlier, after obtaining the experimental data we proceeded with numerical simulations providing with preload of 2500 N onto the model in ANSYS, and the natural frequencies were measured and compared with those without preload, as well as with FFT data in Table 1. The preload had minimal impact on the natural frequencies, though this effect may vary with different materials or mounts.

Table 1. Natural frequencies from both numerical simulation and experiment.

Mode	No-Pre Load (Hz)	Pre-Loaded (Hz)	Experiment (Hz)
1	12.6	12.3	16
2	27.7	18.8	23.7
3	30.7	28	32.1
4	42.6	32.4	45.2
5	49.3	39.1	51.6
6	58.2	50.7	64.4
7	72.3	65	74.4
8	81.7	71.8	80
9	98.2	88.6	96.6
10	102.5	90.7	114

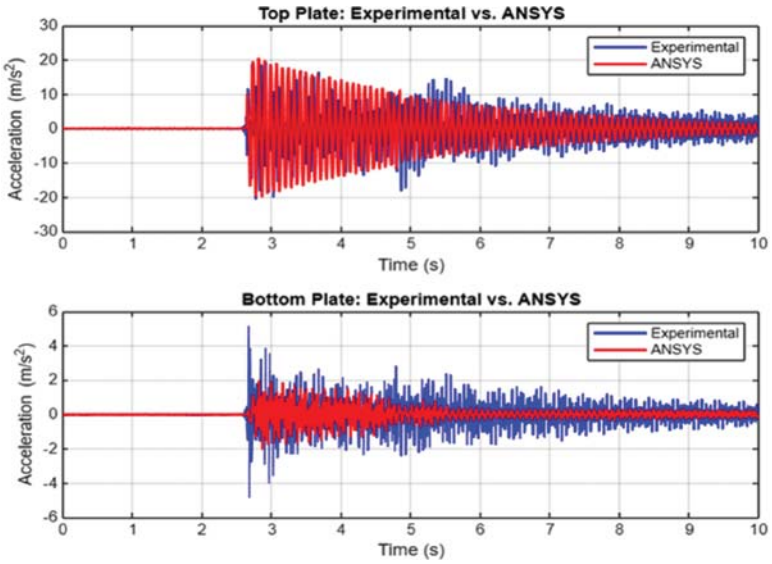

Fig. 5. Top and bottom plate vibration result comparisons.

Fig. 5 shows the transient analysis response plot, showing good agreement between experimental and ANSYS results. The top plate response in both cases was similar, confirming accurate system modelling. Discrepancies in the bottom plate data suggest the need for model refinement, possibly due to boundary conditions or simplifications, to improve accuracy in future work.

The comparison between experimental data and ANSYS simulation shows a reasonable agreement, the alignment is adequate to validate the model. This suggests that the ANSYS model represents the physical system reasonably well. Therefore, the harmonic analysis results from this model can be trusted for further analysis.

Fig. 6 illustrates the insertion loss up to 1500 Hz, offering insights into the performance of the vibration isolators informing that the insertion loss was good enough in mitigating the produced vibrations.

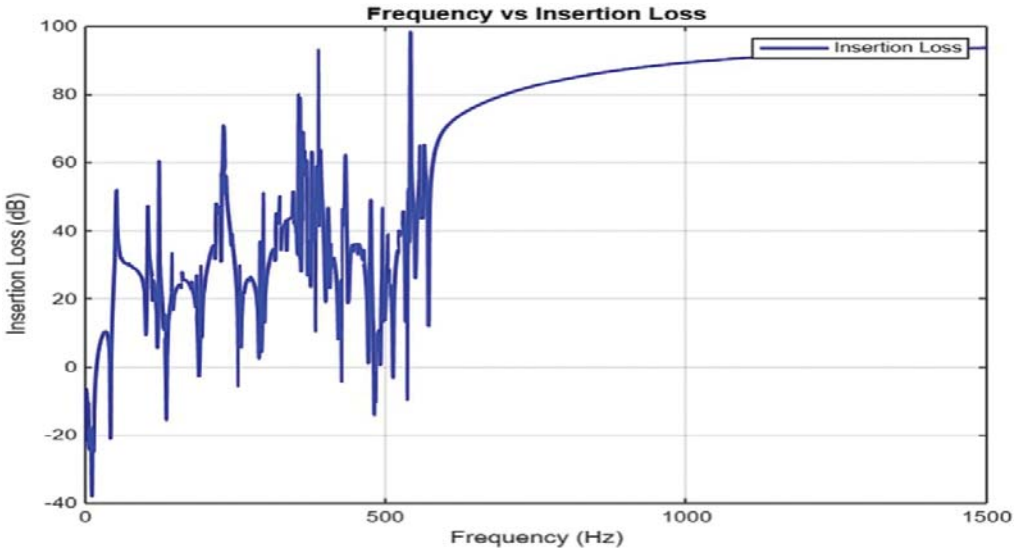

Fig. 6. Plot between Insertion Loss and Frequency obtained through TMM.

5. SUMMARY AND CONCLUSION

This study examined isolator transfer matrices and their effectiveness using insertion loss. Both experimental and numerical investigations produced comparable results.

The experimental work and ANSYS numerical simulations are found to be in good agreement. Predictive Analysis can be done through Finite element analysis to understand the isolator performance with consistent results from the matrix method. For a multiple isolator system, the performance of the isolation provided can be understood through insertion loss. At higher frequencies, the performance of isolator may get reduced due to isolator resonances. These insights are crucial for improving isolator performance in noise and vibration engineering.

REFERENCES

[1] Molloy C. T., 1957. Use of Four-Pole Parameters in Vibration Calculations, *Journal of the Acoustical Society of America,* **29**(7), 842-853.

[2] Snowdon J. C., 1971. Mechanical Four-pole Parameters and Their Application, *Journal of Sound and Vibration,* **15**(3), 307-323.

[3] Munjal M. L., 2014. *Acoustics of Ducts and Mufflers,* John Wiley and Sons, West Sussex, 2nd Edition.

[4] Dickens J. D. and Norwood C. J., 2001. Universal Method to Measure Dynamic Performance of Vibration Isolators under Static Load, *Journal of Sound and Vibration,* **244**(4), 685-696.

[5] Dickens J. D., 2000. Methods to Measure the Four-Pole Parameters of Vibration Isolators, *Acoustics Australia,* **28**(1), 15-21.

[6] Kim S. and Singh R., 2001. Multi-Dimensional Characterization of Vibration Isolators over a Wide Range of Frequencies, *Journal of Sound and Vibration,* **245**(5), 877-913.

[7] Kim S. and Singh R., 2003. Examination of some vibration isolator models and their effects on Vibration and Structure-borne Noise Transmission, *SAE transactions,* pp. 1702-1712.

[8] Sun Shishuo, David W. Herrin and John Baker, 2015. Determination of the Transfer Matrix for Isolators Using Simulation with Application to Determining Insertion Loss, *SAE International Journal of Materials and Manufacturing,* **8**(3), 946-952.

[9] Ungar E. E., 2007. Use of Vibration Isolation, *Handbook of Noise and Vibration Control,* ed. Crocker M. J., John Wiley and Sons, New Jersey.

[10] Izak G. D., 1993. *Vibration Isolation, Noise and Vibration Control in Vehicles,* ed. Crocker M. J. and Ivanov, N. I., Politekhnika, St. Petersurg.

The Journal of Acoustical Society of India : Vol. 52, No. 2, 2025 (pp. 63-70)

Vibration minimization in hydroelectric turbogenerator rotor system using generator support design

Nihar Ranjan Sahoo, Jyothula H. Narayana Rao and J. Srinivas*
Department of Mechanical Engineering, NIT Rourkela, India
e-mail: srinivasj@nitrkl.ac.in

[Received: 30-07-2025; Accepted: 22-08-2025]

ABSTRACT

Noise levels in vertical turbo-generator rotors of hydroelectric power stations are usually in very high decibels and sometimes may lead to final catastrophic failures during critical operating conditions. Simple design modifications can reduce the vibration and noise levels considerably. Hydroelectric vertical rotor system contains a turbine runner shaft at lower end coupled to a generator rotor with various intermediate support bearings. The main centre of noise is noticed at the generator, which is induced by the unbalance and magnetic pull loads along with other coupled system vibrations. Present work focuses on the dynamic analysis of the coupled rotor-bearing system subjected to important nonlinear forces. The equations of motion are formulated, and the transient vibration response is obtained. Further, in order to minimize the vibrations and noise levels at the generator house, a support system for the generator rotor is designed with linear spring elements. The resultant system analysis is conducted and effectiveness of the study is illustrated in detail.

1. INTRODUCTION

Hydroelectric power plants are the third largest renewable energy generators producing several mega-watts of power through the day. The vertical turbo-generator rotor is the main component of the unit. Due to heavy weight of the rotor system, it is always subjected to different types of faults. Mainly, the generator portion even if it is supported over the upper and lower bearings, it acquires magnetic pull-in loads and unbalance excitations during its rotation. This results in continuous high amplitude vibrations resulting in huge noise levels. Measurement of acoustic signal at the generator disk provides vital information about the system condition[1]. Sometimes, analytical modelling of the system also gives a reliable vibration and acoustic data very conveniently. It avoids the collection of field measurements and experimental work.

There are several articles in literature reported the experimental and dynamic modelling of turbo-generator vertical rotor bearing system. Zeng *et al.*[2] illustrated the simplified two mass equivalent vertical turbo-generator rotor system. Here only the unbalance forces were considered. Xu *et al.*[3] made a nonlinear fractional-order mathematical model of the shaft system of a hydro-turbine-generator unit system and introduced the fractional-order damping forces and the fractional-order oil-film forces to the mathematical model of the system, nonlinear dynamical behaviours of system with six fractional orders. Here, the magnetic pull-in forces were also accounted at the generator. Rotor misalignment is a problem that multi-

span rotor systems confront due to poor foundation, installation errors, and shaft deformation. Nikola Kopoulos and Papadopoulos[4] examined the connection between bearing wear depth, misalignment angles and friction force for bearings prior to indicating excessive wear, eccentricity and misalignment. The fault was classified into three types based on its geometric relationship between the centrelines of two shafts: parallel, angular and hybrid misalignments. Hussain and Redmond[5] investigated how two rotors coupled by a rigid coupling responded lateral and torsional to parallel misalignment. Huang *et al.*[6] created a dynamic model to represent a rotor system with rub-impact and misalignment. A numerical integration approach was used to examine the dynamic behaviour of this system. Andres[7] examined the impact of static misalignment angles on the operation of a water-lubricated five-recess hydrostatic journal bearing. Sudhakar and Sekhar *et al.*[8] discussed the consequences of misalignment, condition monitoring methods and different coupling modeling tools. Recently Shi *et al.*[9] presented angular misalignment model of hydroelectric turbo-generator vertical rotor system subjected to different nonlinear forces. Towards identification of fault, here the signal de-noising and holographic approach were also presented.

The vibration and noise control is the primary objective in such power stations. There are several passive, semi-active and active control methods available in the control. However, all these methods require enormous external power during the control action. Recently proposed method of applying axial load on the rotating shaft[10] was one effective method for vibration amplitude control. Shi and Jhou[11] illustrated a multistage signal denoising approach for guide bearing recorded data in hydropower unit. Also, sometimes by supporting properly the motors / generators, it is possible to minimize the vibration and noise. From above literature review, it is noticed that an accurate model of rotor system is essential for vibration / noise control. Present work employs an equivalent four degree of freedom dynamic model of the turbo-generator rotor by considering nonlinear bearing forces, magnetic pull-in loads, with unbalance and misalignment in the rotor system. The equations are solved numerically using fourth order Runge-Kutta method and the dynamic response at the generator rotor is obtained at different speeds of operation and misalignment angles. In order to reduce the amplitudes of oscillation at the generator, an isolator is designed with two radial isolation stiffness forces. The vibration levels have considerably reduced. The remaining part of the paper has three sections: section-2 gives the mathematical modelling and methodology employed. Section-3 presents brief results and discussion and section-4 summarizes and gives conclusions of the work.

2. MATHEMATICAL MODELING

Fig. 1 shows the vertical rotor of turbo-generator system supported on three guide bearings. There is a slight misalignment (angle ϕ) at the coupling.

If m_1, m_2 are the equivalent masses of generator and turbine disks, the equations of motion in x and y directions can be written in terms of equivalent stiffness and damping coefficients as[12]:

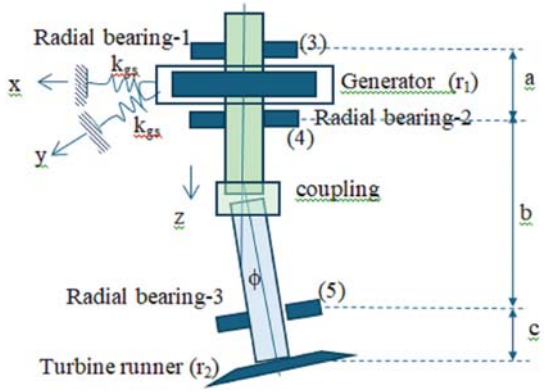

Fig. 1. Vertical rotor bearing system (with supported generator).

$$\begin{cases} m_1\ddot{x}_1 + c_1\dot{x}_1 + K_1x_1 = F_{xg} \\ m_1\ddot{y}_1 + c_1\dot{y}_1 + K_1y_1 = F_{yg} \\ m_2\ddot{x}_2 \mid c_2\dot{x}_2 \mid K_2x_2 = F_{xt} \\ m_2\ddot{y}_2 + c_2\dot{y}_2 + K_2y_2 = F_{yt} \end{cases} \quad (1)$$

where, x_1, y_1, x_2, y_2 are respectively displacements at masses m_1 and m_2.

$$F_{xg} = F_{ump-x} + F_{xbu} + F_{xbl} + m_1e_1\omega^2 \cos \omega t + k_{gs}x_1 \quad (2)$$

$$F_{yg} = F_{ump-y} + F_{ybu} + F_{ybl} + m_1e_1\omega^2 \sin \omega t + k_{gs}y_1 \quad (3)$$

$$F_{xt} = F_{xbt} + m_2e_2 \cos \phi\, \omega^2 \cos(\omega t + \varphi) \quad (4)$$

$$F_{yt} = F_{ybt} + m_2e_2 \cos \phi\, \omega^2 \sin(\omega t + \varphi) \quad (5)$$

are the external forces in x and y directions at the generator and turbine runner respectively. Here, at the generator F_{ump} refers to the asymmetric magnetic pull occurring with stator-rotor magnetic interactions. When the number of the pole pairs of a generator is greater than three, we can get the equations of the asymmetric magnetic pull as[13]:

$$\begin{cases} F_{ump-x} = \frac{R_rL_r\pi K_j^2I_j^2}{4\mu_0}(2\Lambda_0\Lambda_1 + \Lambda_1\Lambda_2 + \Lambda_2\Lambda_3)\cos\emptyset_1 \\ F_{ump-y} = \frac{R_rL_r\pi K_j^2I_j^2}{4\mu_0}(2\Lambda_0\Lambda_1 + \Lambda_1\Lambda_2 + \Lambda_2\Lambda_3)\sin\emptyset_1 \end{cases} \quad (6)$$

where, the four intermediate variables are:

$$\begin{cases} \Lambda_0 = \frac{\mu_0}{\delta_0}\frac{1}{\sqrt{1\ \ \varepsilon^2}} \\ \Lambda_1 = \frac{2\mu_0}{\delta_0}\frac{1}{\sqrt{1-\varepsilon^2}}\left(\frac{1-\sqrt{1-\varepsilon^2}}{\varepsilon}\right) \\ \Lambda_2 = \frac{2\mu_0}{\delta_0}\frac{1}{\sqrt{1-\varepsilon^2}}\left(\frac{1-\sqrt{1-\varepsilon^2}}{\varepsilon}\right)^2 \\ \Lambda_3 = \frac{2\mu_0}{\delta_0}\frac{1}{\sqrt{1-\varepsilon^2}}\left(\frac{1-\sqrt{1-\varepsilon^2}}{\varepsilon}\right)^3 \end{cases} \quad (7)$$

Here, R_r is the generator radius, L_r is its length, δ_0 is the uniform air gap; $\varepsilon = \frac{r}{\delta_0}$ is the relative eccentricity, μ_0 is the magnetic permeability of the air; K_j is the coefficient of fundamental magnetomotive force of air gap; I_j is the exciting current of the generator. Within the bearings, it is assumed that the fluid is incompressible and its viscosity is constant across the fluid. Non-linear oil-film forces based on the assumption of short bearings (F_{xb}, F_{yb}) can be expressed as:

$$\begin{bmatrix} f_{xb} \\ f_{yb} \end{bmatrix} = \sigma \begin{bmatrix} f_{xb} \\ f_{yb} \end{bmatrix} \quad (8)$$

where

$$\sigma = \eta\omega\left(\frac{D}{2}\right)L\left(\frac{D}{2c}\right)^2\left(\frac{L}{D}\right)^2 \quad (9)$$

is called modified Sommer field's number. Here η represents lubricant viscosity; L, D and c are bearing length, bearing diameter and bearing radial clearance respectively. The non-dimensional bearing force components are given as[14].

$$\begin{bmatrix} f_{x0} \\ f_{y0} \end{bmatrix} = \frac{\sqrt{(x-2y)^2+(y+2x)^2}}{1-x^2-y^2} \times \begin{bmatrix} 3xV(x,y,\alpha) - \sin\alpha\, G(x,y,\alpha) - 2\cos\alpha\, S(x,y,\alpha) \\ 3yV(x,y,\alpha) + \cos\alpha\, G(x,y,\alpha) - 2\sin\alpha\, S(x,y,\alpha) \end{bmatrix} \quad (10)$$

$$V(x,y,\alpha) = \frac{(2 + y\cos\alpha - x\sin\alpha)\, G(x, y, \alpha)}{1 - x^2 - y^2} \quad (11)$$

$$S(x,y,\alpha) = \frac{x\cos\alpha + y\sin\alpha}{1-(x\cos\alpha + y\sin\alpha)^2} \quad (12)$$

The functions *V*, *S*, *G* and α are respectively given as:

$$G(x,y,\alpha) = \frac{2}{\sqrt{1-x^2-y^2}}\left[\frac{\pi}{2} + \tan^{-1}\left(\frac{y\cos\alpha - x\sin\alpha}{\sqrt{1-x^2-y^2}}\right)\right] \tag{13}$$

$$\alpha = \tan^{-1}\left(\frac{y+2\dot{x}}{x-2\dot{y}}\right) - \frac{\pi}{2}\,sign\left(\frac{y+2\dot{x}}{x-2\dot{y}}\right) - \frac{\pi}{2}\,sign(y+2\dot{x}) \tag{14}$$

There are three bearing locations, whose *x* and *y* coordinates are obtained from their radial displacement and geometric relations as $r_3 = \frac{2(a+b+c)r_2 - ar_2}{a+2b+2c}$, $r_4 = \frac{2(b+c)r_2 + ar_2}{a+2b+2c}$ and $r_5 = \frac{2cr_2 + (a+2b)r_2}{a+2b+2c}$. Here $r_1 = \sqrt{x_1^2 + y_1^2}$ and $r_2 = \sqrt{x_2^2 + y_2^2}$ are the radial displacements at the generator and turbine runner respectively. The equivalent stiffness of generator and turbine shafts is given in terms of the bearing stiffness coefficients k_1, k_2 and k_3 as:

$$K_1 = (2k_{11} + \frac{r_2}{r_1}k_{12}) \tag{15}$$

$$K_2 = (2k_{22} + \frac{r_2}{r_2}k_{12}) \tag{16}$$

Where

$$k_{11} = \frac{2k_1(a+b+c)^2 + 2k_2(b+c)^2 + 2k_3c^2}{(a+2b+2c)^2} \tag{17}$$

$$k_{12} = \frac{2(ak_2(b+c) + ck_3(a+2b) - ak_1(a+b+c))}{(a+2b+2c)^2} \tag{18}$$

$$k_{22} = \frac{k_1a^2 + k_2a^2 + k_3(a+2b)^2}{(a+2b+2c)^2} \tag{19}$$

Here, *a*, *b* and *c* are respectively the distances between the top two bearings, bottom two bearings and turbine runner and turbine bearing. The shaft misalignment is considered at the coupling with misalignment angle ϕ.

3. RESULTS AND DISCUSSIONS

A computer program is developed to solve the four dynamic eqs. (1) to obtain the response of the system. Frequency spectra are obtained using fast Fourier transforms at different speeds of operation. Further, the misalignment angle is varied and the amplitudes at the generator disk are observed without any generator support system. The following input parameters are considered for illustrating the methodology[2]:

a = 4m, b = 3 m, c = 1.2 m, $m_1 = 7.32 \times 10^5$ kg, $m_2 = 2.4 \times 10^5$ kg, $c_1 = 0.35\ 10^7$ Ns/m, $c_2 = 0.25\ 10^7$ Ns/m, $k_1 = 0.2 \times 10^9$ N/m, $k_2 = 0.2 \times 10^9$ N/m, $k_3 = 0.35 \times 10^9$ N/m, $e_1 = 1.0$ mm, and $e_2 = 0.5$ mm, bearing parameters are: length = 10 mm, diameter = 25 mm, radial clearance = 0.3 mm and viscosity of oil = 0.04 m^2/s. At the generator rotor, the uniform air gap $\delta_0 = 0.008$ m, $L_r = 0.5$m, radius R = 1.2 m, $K_j = 0.05$, $\mu = 4\pi \times 10^{-7}$ H/m and current $I_j = 1000$ amp. Figures 2 to 4 show the generator rotor time and frequency responses at three different speeds of operation namely 150 rpm, 500 rpm and 800 rpm with 5 degree angular misalignment.

It is clearly noticed from sub-synchronous vibration in frequency spectra that as speed increases, the fundamental frequency along with amplitude. In all the frequency diagrams, there is a dominant first order engine resonance (1x). The effect of misalignment angle on the generator vibration response is shown in Fig. 5. It is seen that angular misalignment increases the fundamental frequency and amplitudes. However, after some value of misalignment, the amplitude increase is not considerable.

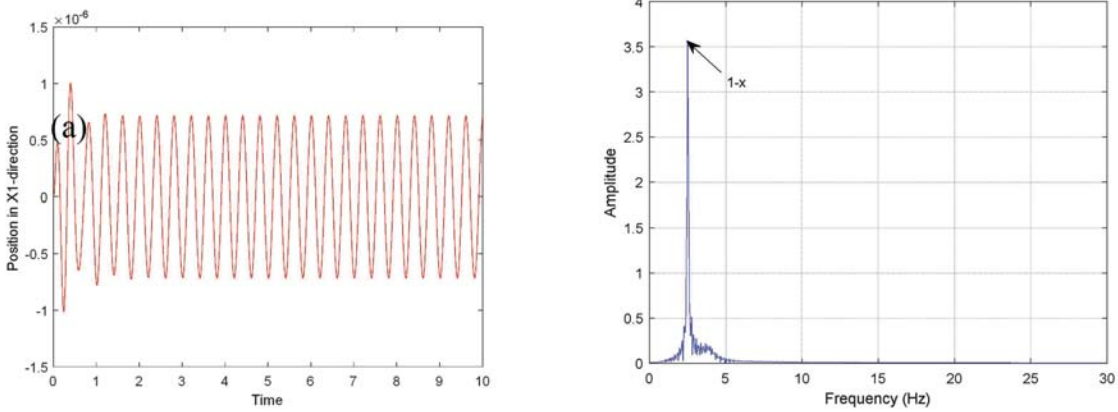

(a) Time response (b) Frequency spectrum

Fig. 2. Displacement at generator (150 rpm).

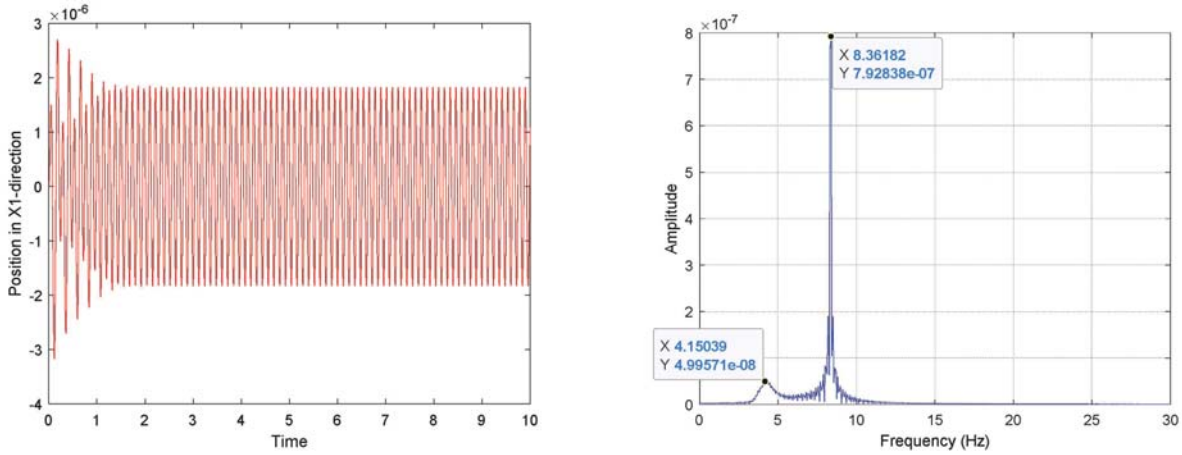

(a) Time response (b) Frequency spectrum

Fig. 3. Displacement at generator (500 rpm).

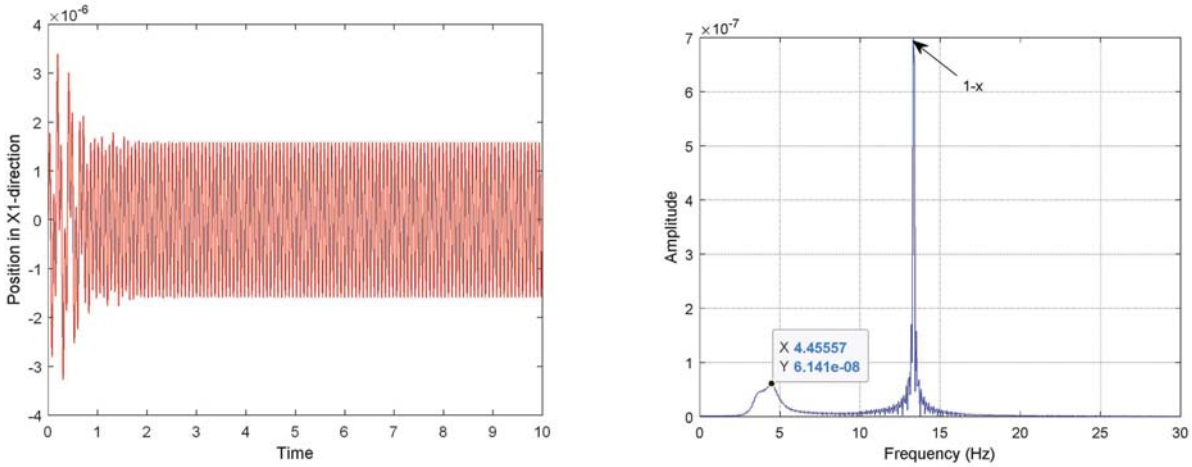

(a) Time response (b) Frequency spectrum

Fig. 4. Displacement at generator (800 rpm).

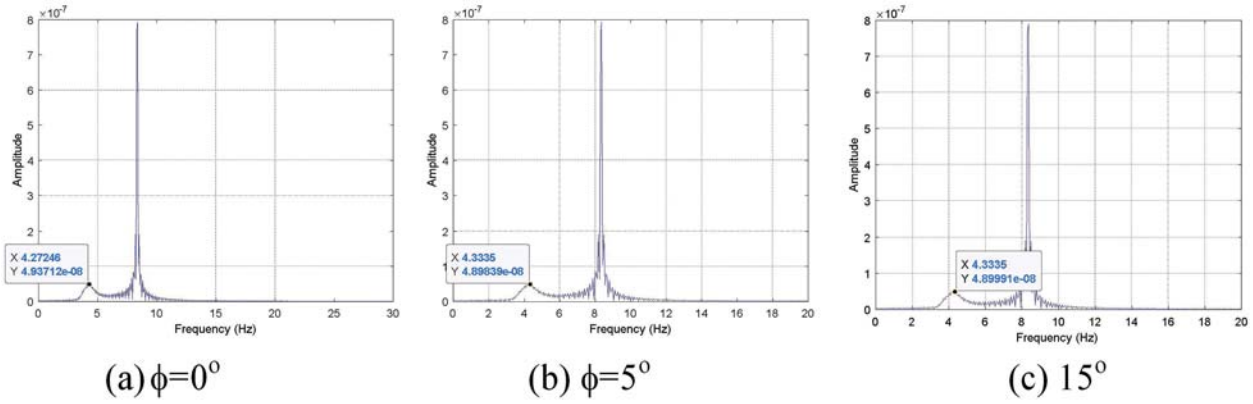

Fig. 5. Effect of misalignment on the output amplitudes at 500 rpm.

Fig. 6 shows the effect of misalignment at three different speeds namely 500 rpm, 900 rpm and 1200 rpm. It is noticed that effect of misalignment is not considerable at these speeds.

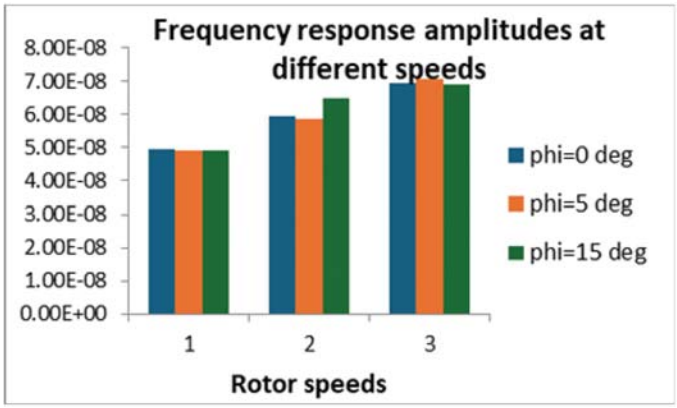

Fig. 6. Misalignment angle effect at different operating speeds.

Effect of armature current at the generator on the vibration response is illustrated in Fig.7 at 900 rpm. It is interestingly seen that up to certain value of current, the amplitude increases, later-on it decreases.

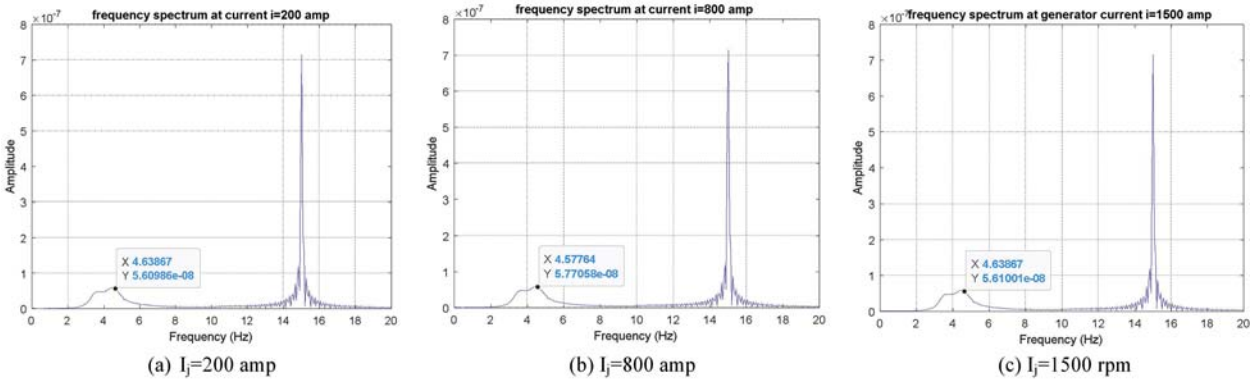

Fig. 7. Effect of armature current.

Finally, in order to minimize the vibration amplitudes, the generator rotor support system with stiffness kgs=1 10^{11} N / m is considered. Fig.8 shows the amplitude reduction relative to unsupported generator rotor.

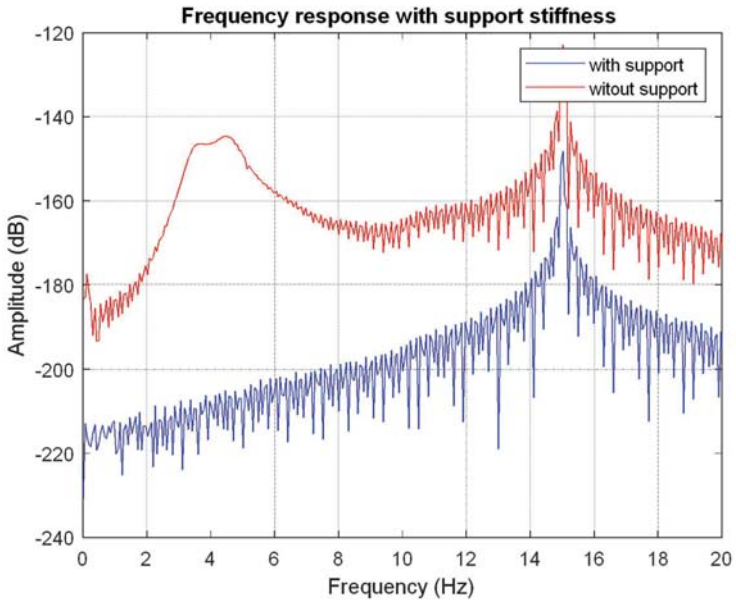

Fig. 8. Vibration reduction using a support box for generator.

The vibration reduction occurred at the system natural frequency considerably. Therefore, in order to minimize the vibration and noise levels, it is recommended to use a support for the rotor at appropriate places in addition to the guide bearings.

4. CONCLUSIONS

This work presented the dynamic analysis of rotor-bearing system of hydroelectric turbo-generator system by accounting various common nonlinearities. Computer simulation studies were conducted using interactive computer program to perform several parametric studies. Effect of operating speed, misalignment angle, and generator-armature current on the vibration amplitudes was studied thoroughly. By supporting the generator rotor flexibly, it was shown that the vibration amplitudes can be considerably reduced. In future work, the vibration and acoustic signature recorded at the generator location may be further used to predict the faults in the rotor.

REFERENCES

[1] F. Dao, Y. Zeng, Y. Zou, X. Li and J. Qian, 2021. Acoustic vibration approach for detecting faults in hydroelectric units: A review, *Energies,* **14**(23), 10.3390 / en14237840

[2] Y. Zeng, L. Zhang, Y. Guo, J. Qian and C. Zhang, 2014. The generalized Hamiltonian model for the shafting transient analysis of the hydro turbine generating sets. *Nonlinear Dyn.,* **76,** 1921-1933.

[3] B. Xu, D. Chen, H. Zhang and R. Zhou, 2015. Dynamic analysis and modelling of a novel fractional-order hydro-turbine-generator unit. *Nonlinear Dyn.,* **81,** 1263-1274.

[4] P.G. Nikolakopoulos and C.A. Papadopoulos, 2008. A study of friction in worn misaligned journal bearings under severe hydrodynamic lubrication. *Tribol Int .,* **41,** 461-72.

[5] K.M.Al. Hussain and I. Redmond, 2002. Dynamic response of two rotors connected by rigid mechanical coupling with parallel misalignment, *J. Sound Vib.,* **249**(3), 483-498.

[6] H. Zhiwei, Z. Jianzhong, Y. Mengqi and Z. Yongchuan, 2011. Vibration characteristics of a hydraulic generator unit rotor system with parallel misalignment and rub- impact, *Arch. Appl. Mech.*, **81**(7), 829-838.

[7] LAS Andres, 1993. The effect of journal misalignment on the operation of a turbulent f low hydrostatic bearing. *ASME J Tribol .*, **115,** 355-63.

[8] G.N.D.S. Sudhakar and A.S. Sekhar, 2009. Coupling misalignment in rotating machines: modelling, effects and monitoring, *Noise Vibration Worldwide,* **40**(1), https: / / doi.org / 10.1260 / 0957-4565.40.1.17

[9] Y. Shi, J. Huang, Y. Xi and B. Liu, 2022. A vibration fault identification framework for shafting systems of hydropower units: Nonlinear modelling, signal processing and Holographic identification, *Sensors,* **22,** 4266. doi.org / 10.3390 / s22114266.

[10] L. Ran, D. Halim, C.K. Thein and M. Galea, 2024. Lateral vibration attenuation of a rotor system using an axial control mechanism with resonance detuning, *Mech. Systems & Signal processing,* **211,** 111220.

[11] Y. Shi and J. Zhou, 2021. Multistage noise reduction processing for vibration signal of hydropower units, *J. Physics: Conf. Series,* **2108,** 012008.

[12] Y. Shi, J. Zhou, X. Lai, Y. Xu, W. Guo and B. Liu, 2021. Stability and sensitivity analysis of the bending-torsional coupled vibration with the arcuate whirl of hydro-turbine generator unit, *Mech. Systems and Signal Processing,* **149,** 107306.

[13] J. Zhang, L. Zhang, Z. Ma, X. Wang, Q. Wu, and Z. Fan, 2021. Coupled bending-torsional vibration analysis for rotor-bearing system with rub-impact of hydraulic generating set under both dynamic and static eccentric electromagnetic excitation, *Chaos, Solitons, Fractals,* **147,** 110960.

[14] L. Xiang, Y. Zhang, A. Hu and F. Ye, 2020. Dynamic analysis and experiment investigation of a cracked dual-disc bearing-rotor system based on orbit morphological characteristics, *Applied Mathematical Modeling,* **80,** 17-32.

The Journal of Acoustical Society of India : Vol. 52, No. 2, 2025 (pp. 71-77)

Vibration / Noise reduction in multi-rotor drones using optimal phase synchronization method

Bipllab Chakraborty, J.Srinivas and Chikesh Ranjan
NIT Rourkela, Rourkela-769 008, India
e-mail: chakrabortybipllab012@gmail.com

[Received: 30-07-2025; Accepted: 22-08-2025]

ABSTRACT

Using drones for various purposes has sparked concerns about the noise they create. There are several techniques to mitigate the drone noise such as propeller geometrical changes, material modifications, and active control using additional speakers. Recently the concept of phase synchronization with multiple propellers has drastic effect in reducing drone noise. In phase synchronization, the rotors are turned at the same rpm yet have a clear angular phase difference in position. If the angular phase difference is properly adjusted, the noise waves or vortices generated by every rotor destructively interfere with themselves. This makes the total noise from the drone to decrease remarkably, particularly at the dominant frequency of the blade passing and its harmonics. This paper presents a comprehensive approach to reduce the noise / vibration produced by drone propellers without affecting the thrust. By considering the overall dynamics of the quad rotor drone with phase differences in thrust produced by each rotor, initially, the vibration responses are obtained numerically. The amplitudes of vibration in yaw direction are further minimized by setting the optimum relative phase angles subjected to a minimum thrust constraint. The dynamic response and noise levels of the effective phase angle configuration are finally reported.

1. INTRODUCTION

The developing field of unmanned aerial vehicles, more commonly known as drones, has taken off in the last decade, with applications in many areas, including agriculture, logistics, surveillance, and entertainment. As one might praise the technological advances in the design and autonomy of drones for various mission tasks, a potential big challenge of multi-rotor drones is the resulting noise produced due to vortex shedding created by rotor propellers. The sound produced by the unmanned aerial vehicle (UAV) cannot be used in such places where privacy is important or where surveillance is the prime concern. The sound produced by the rotors of the multirotor UAV is a mixture of propeller sound and other external sounds. Generally, separating the two sounds and analyzing them using a noise cancellation strategy is very difficult. Noise Cancellation is a technology that reduces unwanted background noise. There are mainly two basic types of cancellation methods which are active and passive noise cancellation. Active noise cancellation (ANC) employs electronics to fight ambient noise. Sound waves are processed by a chip and subsequently produce an appropriate 'anti-noise' wave. The anti-noise wave is generated by the device's speaker and blocks out the original noise.

In passive noise cancellation, the physical design and material of the component would matter. Based on the research work of Go and Choi[1], a new methodology was proposed for ground sound detection via a drone with microphone arrays attached to it. Experiments have confirmed that the system can accurately determine the source of sound within 10 degrees after an explosion has occurred. Wang *et al.*[2] showed a new microphone array system combining filtering and separation techniques to effectively reduce a drone's noise while capturing target sounds, achieving better performance and real-time processing for future embedded applications. Salvati *et al.*[3] focused on the localization of sound sources using microphone arrays at the onboard drones. Here, the drone noise challenges were presented using a unique beam-forming technique, keeping the microphone array away from the propellers. Sulimoy *et al.*[4] showed that, with a high-quality oscillator, a centralized drone network sync method with a 1-20 second signal confines the errors to sub-1.5 nanoseconds, thus helping in aerial sensor applications. Roger *et al.*[5] presented models of the sound from small drone propellers using analytical formulae, including forward flight and mounting effects, targeting fast noise prediction tools for low-noise design and noise impact assessment. Iqbal *et al.*[6] used a 4-microphone array and signal processing techniques to perform high-accuracy localization and passive UAV detection using sound signature analysis, opening perspectives toward real-time assessment and tracking. Lee *et al.*[7] identified that closing the rotors in multi-rotor drones' decreases thrust and increases force oscillations leading to more noise due to complex wake interaction. Experiments conducted by Yu *et al.*[8] shown that the noise of a drone could be minimized by variable pitch control in its rotors due to steadier rotation and more optimized phases of the blades. Narine[9] illustrated that with active noise cancellation using sound wave analysis and phase adjustment, the noise reduced by 43.82% in drones. The blade phase angle was found to be a major factor influencing noise reduction in synchronized propellers. Turhan *et al.*[10] have shown that an optimum phase angle of 90 degrees reduces the maximum noise, particularly tonal noise, and overall sound pressure level, especially under inflow conditions. They considered the possibility of using phase synchronization to decrease multi-rotor aircraft noise. Guan *et al.*[11] considered the phase synchronization for noise minimization in quadrotors. Computer simulations proved that this technique can considerably reduce noise levels in the case of a single point of observation and separate areas, which confirms the possibility of its practical application. Schiller *et al.*[12] described the application of phase synchronization to reduce multiple-rotor noise. Experiments and simulations demonstrated that relative phase control of rotors significantly reduced noise levels, especially at the blade passage frequency. Sun *et al.*[13] illustrated that optimizing the blade angles also affects the noise reduction considerably. Valente *et al.*[14] proposed an algorithm for drone propeller synchronization based on motor speed adjustment concerning real-time propeller position and a desired position and validated with experiments under high-speed and real-world flights. Encinas *et al.*[15] showed in their paper an approach for using a specific SSA algorithm for de-noising a single-channel drone noise recording. The average noise reduction was 1.41 decibels, thus giving a clearer desired sound. Despite the above works, there is an urgent need to minimize the quadrotor noise using simple methods like phase synchronization and passive damping approaches. The present work focuses on dynamic modeling and phase synchronization studies in quadrotor drone systems subjected to multiple disturbances. The computer program is developed to solve the dynamic equations with modified thrust relations. The effect of three relative phase angles on the dynamics is studied. An optimization framework is proposed to minimize the vibration amplitudes without losing the total thrust in the system.

2. DYNAMIC MODEL AND METHODOLOGY

A quad copter is essentially a stiff, cross-linked structure with four separate, fixed-pitch propellers on each rotor. As seen in Figure 1, of the four propellers, two opposite ones rotate in a clockwise manner, and the other two in an anti-clockwise direction. Control of the quadcopter is achieved by varying the propellers' angular speed, Ω_i (where i = 1, 2, 3, 4), which is indirectly by changing thrust. The rotary motion of a quad copter can be described by roll (ϕ), pitch (θ), and yaw angles (ψ), about the X, Y, and Z axes, respectively. Every controller input influences a certain movement. The four control inputs to quad rotor for speed adjustment are given by:

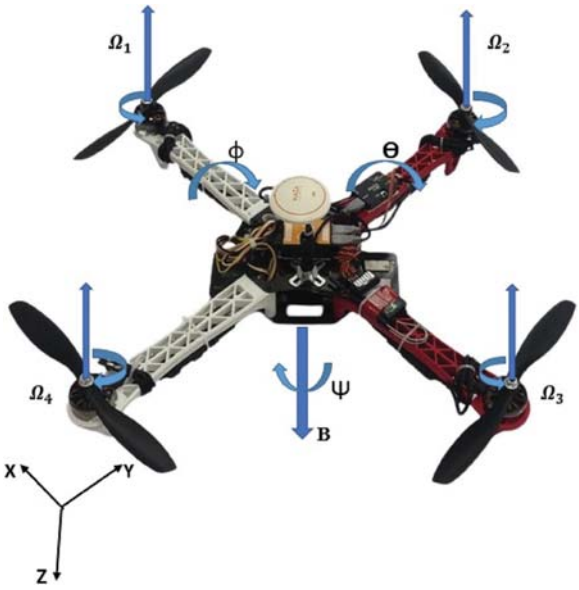

Fig. 1. Quad copter axes nomenclature.

$$u_1 = k_f (\Omega_1^2 + \Omega_2^2\cos\alpha_2 + \Omega_3^2\cos\alpha_3 + \Omega_4^2\cos\alpha_4) \quad (1)$$

$$u_2 = k_f (\Omega_4^2\cos\alpha_4 + \Omega_2^2\cos\alpha_2) \quad (2)$$

$$u_3 = k_f (-\Omega_3^2\cos\alpha_3 + \Omega_1^2) \quad (3)$$

$$u_4 = k_M (-\Omega_1^2 + \Omega_2^2\cos\alpha_2 - \Omega_3^2\cos\alpha_3 + \Omega_4^2\cos\alpha_4) \quad (4)$$

Where k_f and k_M are thrust and moment coefficients respectively, while α_2, α_3 and α_4 are the relative phase angles at motors 2, 3, and 4 with respect to motor-1 respectively. The complete dynamic model of the quadcopter is described in Eqs. (5)-(10).

$$\ddot{X} = \frac{1}{m}\left[-k_{t_x}\dot{X} + u_1(\sin\theta\sin\Psi + \cos\theta\cos\Psi\sin\theta)\right] \quad (5)$$

$$\ddot{y} = \frac{1}{m}\left[-k_{t_y}\dot{y} + u_1(-\sin\theta\cos\Psi + \cos\theta\sin\Psi\sin\theta)\right] \quad (6)$$

$$\ddot{Z} = \frac{1}{m}\left[-k_{t_z}\dot{Z} - mg + u_1(\cos\Psi\cos\theta)\right] \quad (7)$$

$$\ddot{\phi} = \dot{p} = \frac{1}{I_x}\left[-k_{r_x}p + lu_2 + (I_y - I_z)qr - I_r q\omega_r\right] \quad (8)$$

$$\ddot{\theta} = \dot{q} = \frac{1}{I_y}\left[-k_{r_y}q + lu_3 + (I_Z - I_x)pr - I_r p\omega_r\right] \quad (9)$$

$$\ddot{\Psi} = \dot{r} = \frac{1}{I_Z}\left[u_4 - k_{r_z}r + (I_x - I_y)pq\right] \quad (10)$$

Here, l is arm length, I_x, I_y, I_z are moments of inertia, k_{tx}, k_{ty}, k_{tz}, k_{rx}, k_{ry}, k_{rz} are respectively the aerodynamic thrust and moment drag coefficients. Thus, four control inputs can characterize the quad copter's entire dynamic model. $u=[u_1\ u_2\ u_3\ u_4]^T$ and there are 12 state vectors, $x_s = [x\ y\ z\ \dot{x}\ \dot{y}\ \dot{z}\phi\theta\square\ \psi\ p\ q\ r]^T$. Phase control, or phase synchronization states that the propellers are synchronized (i.e., rotating at equivalent rates) and relies on changes to the relative azimuthal blade position, or phase, to minimize the blade passing frequency noise radiated in specific directions.

To the above end, the current study examines optimal phase synchronization methodology as a new means to provide decreased noise levels within multi-rotor drones. It is assumed that by closely controlling the phase angles between the rotors at a relatively even proportion to one another, there will be better assured destructive interference patterns which lead to a decreased overall noise / vibration emissions. The optimization formulation is described below

$$\text{Minimize } f(X)$$

$$\text{Subjected to}$$

$$\text{thrust} \geq \text{minimum thrust}$$

$$X_{min} \leq X \leq X_{max} \tag{11}$$

where f(X) is the amplitude of vibration response, and X is the design vector containing 3 relative phase angles. At the same time, X_{min} and X_{max} are the minimum and maximum values of phase angles which are 0 and 180 degrees respectively. The total thrust is calculated in every cycle and compared with the minimum value. The entire program is executed with MATLAB optimization toolbox.

3. RESULTS AND DISCUSSION

Table 1[10] displays the quad copter nominal parameters considered in the study.

Table 1. Parametersof quad rotor

Symbol	Description	Value	Unit
I_x	Moments of Inertia	7.5e-3	$kg.m^2$
I_y		7.5e-3	
I_z		15e-3	
l	Arm length	0.23	m
I_r	Inertia of motor of motor	6e-5	$kg.m^2$
k_f	Thrust coefficient	3.13e-5	Ns^2
k_M	Moment coefficient	7.5e-7	Nms^2
m	Mass of quad copter	0.65	Kg
g	Gravity	9.81	ms^2
k_{tx}	Aerodynamic thrust drag coefficient	0.1	Ns/m
k_{ty}		0.1	
k_{tz}		0.1	
k_{rx}	Aerodynamic moment drag coefficient	0.1	Nm.s
k_{ry}		0.1	
k_{rz}		0.1	

Figure 2 shows the quad rotor dynamic response for the zero phase angle setting.

All zero initial conditions are considered. Further, the three phase angle differences in three levels are considered to obtain the maximum vibration level (amplitude) at the same RPM. Using 3-factor-3 level design of experiments, the yaw motion amplitudes for L9 orthogonal array of experiments are reported in Tables 2 and 3.

By regression fitting of the above data, the expression for yaw motion amplitude (y) in terms of the three-phase angle differences in radians (x_1, x_2, x_3) is obtained from MATLAB film function as:

$$y = f(x_1, x_2, x_3) = 1 + 0.1412x_1 - 0.1218x_2 + 0.1117x_3 \tag{12}$$

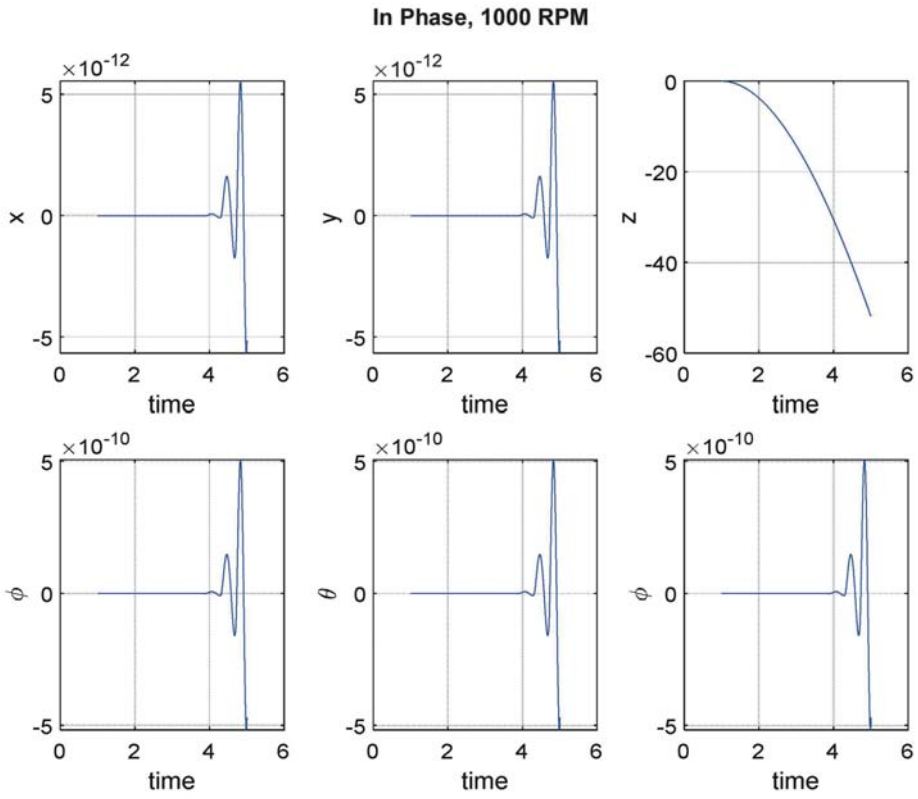

Fig. 2. In-phase condition with 1000 RPM.

Table 2. Combination of parameters (in degrees) and their levels considered.

Phase difference at propeller-2			Phase difference at propeller-3			Phase difference at propeller-4		
A1	A2	A3	B1	B2	B3	C1	C2	C3
10	60	130	30	70	150	50	90	170

Table 3. L9 orthogonal array of experiments.

Exp. No	A (rad)	B (rad)	C (rad)	Yaw motion amplitude (rad)
1	0.1746 (A1)	0.5238(B1)	0.873(C1)	4.935 10^{-2}
2	0.1746 (A1)	B2=1.2223(B2)	1.5714(C2)	7.394 10^{-2}
3	0.1746 (A1)	B3=2.619(B3)	2.968(C3)	2.773 10^{-2}
4	1.0476 (A2)	B1=0.5238(B1)	1.5714(C2)	0.2827
5	1.0476(A2)	B2=1.2223(B2)	2.968(C3)	0.37814
6	1.0476(A2)	B3=2.619(B3)	0.873(C1)	0.00
7	2.2698(A3)	B1=0.5238(B1)	2.968(C3)	0.61469
8	2.2698(A3)	B2=1.2223(B2)	0.873(C1)	0.27779
9	2.2698(A3)	2.619(B3)	1.5714(C2)	0.16078

Now using this function, optimization methodology is adopted to minimize the yaw displacement via PSO(particle swarm optimization) technique, such that the total thrust $Q = \omega^2 + \omega^2 \cos x_1 + \omega^2 \cos x_2 + \omega^2 \cos x_3$ is more than $3\ \omega^2 = 30000$ N in present case.

An experimental work is also attempted to measure the sound pressure level of the quad copter at laboratory level. Fig. 3 shows the time and frequency domain signals of noise level without phase synchronization.

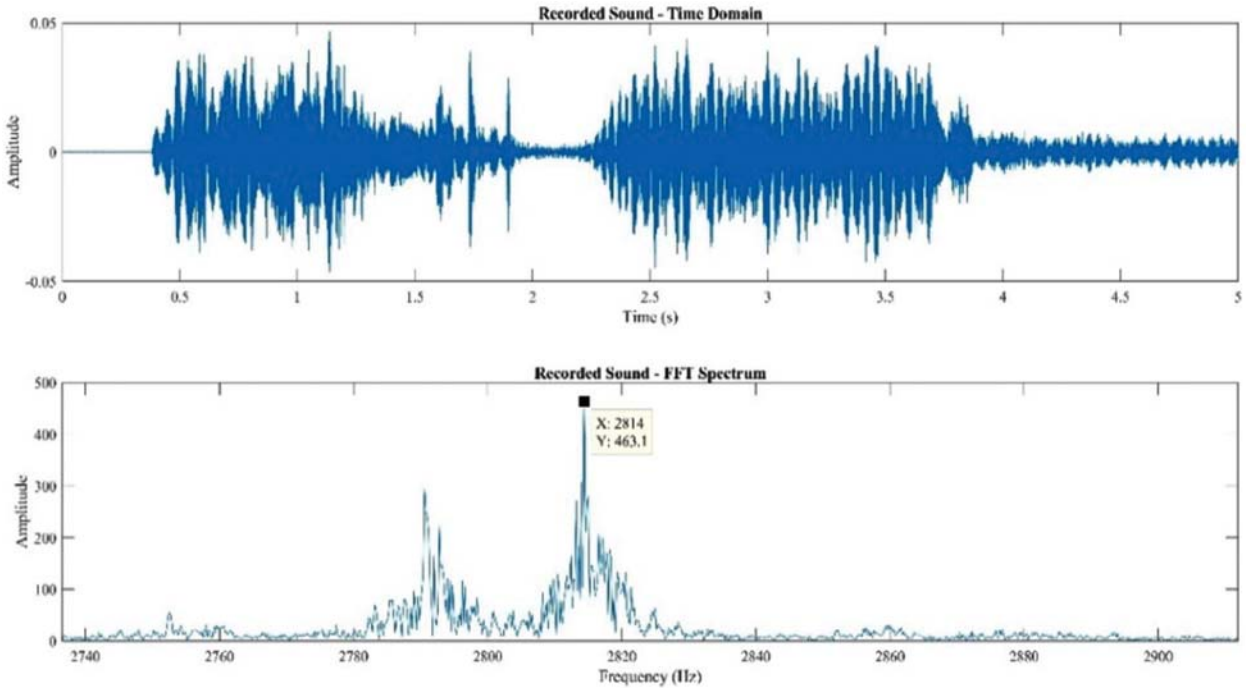

Fig. 3. Amplitude vs Frequency graph at in-phase condition.

Further, another series of experiments are planned with phase synchronization to measure the acoustic response. Fig. 4 shows the experimental set-up employed in the work.

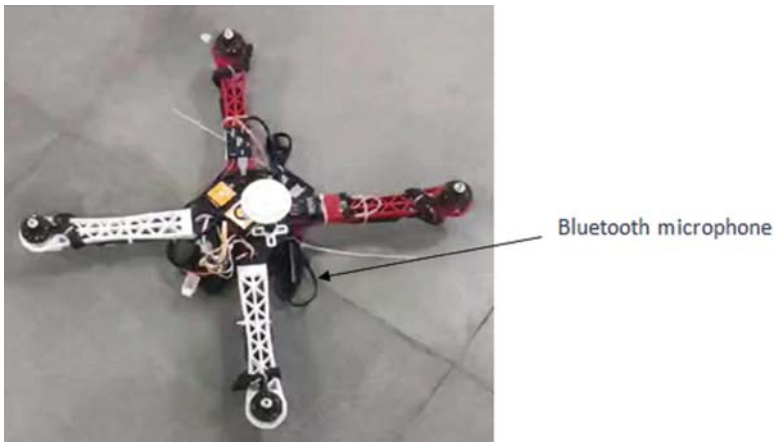

Fig. 4. Quad copter connected to a Bluetooth microphone.

4. CONCLUSION & FUTURE WORK

In this work, the following research offers an integrated approach for vibration / noise reduction in the propellers of drones with no loss in thrust. Considering the overall dynamics of a quad rotor drone having phase differences in thrust provided by each rotor, vibration responses are first obtained

numerically. The amplitudes of vibration are then minimized with the optimization of relative phase angles subjected to a minimum thrust constraint. In the future, more experiments will be conducted to understand in which direction noise levels are minimized. Also, the neural network-based function approximation task is another important target. Theoretical relationship between vibration and noise will be studied for the possible development of a common method for their reduction, using the phase synchronization technique toward an improved quality of life with reduced environmental impact and improved performance in many applications.

REFERENCES

[1] Go Y. J. and Choi J. S., 2021. An acoustic source localization method using a drone-mounted phased microphone array. *Drones,* **5**(3), 75.

[2] Wang L. and Cavallaro A., 2020. A blind source separation framework for ego-noise reduction on multi-rotor drones. *IEEE/ACM Transactions on Audio, Speech, and Language Processing,* **28,** 2523-2537.

[3] Salvati D., Drioli C., Ferrin G. and Foresti G. L., 2019. Acoustic source localization from multirotor UAVs. *IEEE Transactions on Industrial Electronics,* **67**(10), 8618-8628.

[4] Sulimov A. I., Sherstyukov O. N., Latypov R. R. and Nurgaliev D. K., 2021. Simulation of periodic synchronization of UAV's clock. *In 2021 Systems of Signal Synchronization, Generating and Processing in Telecommunications (SYNCHROINFO),* 1-8. IEEE.

[5] Roger M. and Moreau S., 2020. Tonal-noise assessment of quadrotor-type uav using source-mode expansions. *In Acoustics,* **2**(3), 674-690. MDPI.

[6] Iqbal M. A., Zhao Z., Zhi Yong X. and Rehman S. U., 2020. 3-D localization of UAV and detection based on harmonics index and spectral entropy criteria. *In IOP Conference Series: Materials Science and Engineering,* **853**(1), 012037. IOP Publishing.

[7] Lee H. and Lee D. J., 2020. Rotor interactional effects on aerodynamic and noise characteristics of a small multi rotor unmanned aerial vehicle. *Physics of Fluids,* **32**(4).

[8] Yu K., Ko J., Jeong J. and Lee S., 2024. Comparative analysis of multi rotor drone fixed-pitch and variable-pitch control systems: Acoustic characteristics and rotor phase control. *Journal of Sound and Vibration,* **573,** 118187.

[9] Narine M., 2020. Active noise cancellation of drone propeller noise through wave form approximation and pitch-shifting.

[10] Turhan B., Jawahar H. K., Gautam A., Syed S., Vakil G., Rezgui D. and Azarpeyvand M., 2024. Acoustic characteristics of phase-synchronized adjacent propellers. *The Journal of the Acoustical Society of America,* **155**(5), 3242-3253.

[11] Guan S., Lu Y., Su T. and Xu X., 2021. Noise attenuation of a quad rotor using phase synchronization method. *Aerospace Science and Technology,* **118,** 107018.

[12] Schiller N. H., Pascioni K. A. and Zawodny N. S., 2019. Tonal noise control using rotor phase synchronization. *In Vertical Flight Society Annual Forum and Technology Display (VFS Forum 75)* (No. NF1676L-31452).

[13] Sun J., Yonezawa K., Tanabe Y., Sugawara H. and Liu H., 2023. Blade twist effects on aerodynamic performance and noise reduction in a multirotor propeller. *Drones,* **7**(4), 252.

[14] Valente V. T., Johnson E. N. and Greenwood E., 2022. Implementation of a Phase Synchronization Algorithm for Multirotor UAVs. *In 2022 IEEE/AIAA 41st Digital Avionics Systems Conference (DASC),* 1-6. IEEE.

[15] Encinas F. G., Silva L. A., Mendes A. S., González G. V., Leithardt V. R. Q. and Santana J. F. D. P., 2021. Singular spectrum analysis for source separation in drone-based audio recording. *IEEE Access,* **9,** 43444-43457.

INFORMATION FOR AUTHORS

ARTICLES

The Journal of Acoustical Society of India (JASI) is a refereed publication published quarterly by the Acoustical Society of India (ASI). JASI includes refereed articles, technical notes, letters-to-the-editor, book review and announcements of general interest to readers.

Articles may be theoretical or experimental in nature. But those which combine theoretical and experimental approaches to solve acoustics problems are particularly welcome. Technical notes, letters-to-the-editor and announcements may also be submitted. Articles must not have been published previously in other engineering or scientific journals. Articles in the following are particularly encouraged: applied acoustics, acoustical materials, active noise & vibration control, bioacoustics, communication acoustics including speech, computational acoustics, electro-acoustics and audio engineering, environmental acoustics, musical acoustics, non-linear acoustics, noise, physical acoustics, physiological and psychological acoustics, quieter technologies, room and building acoustics, structural acoustics and vibration, ultrasonics, underwater acoustics.

Authors whose articles are accepted for publication must transfer copyright of their articles to the ASI. This transfer involves publication only and does not in any way alter the author's traditional right regarding his/her articles.

PREPARATION OF MANUSCRIPTS

All manuscripts are refereed by at least two referees and are reviewed by the Publication Committee (all editors) before acceptance. Manuscripts of articles and technical notes should be submitted for review electronically to the Chief Editor by e-mail or by express mail on a disc. JASI maintains a high standard in the reviewing process and only accept papers of high quality. On acceptance, revised articles of all authors should be submitted to the Chief Editor by e-mail or by express mail.

Text of the manuscript should be double-spaced on A4 size paper, subdivided by main headings-typed in upper and lower case flush centre, with one line of space above and below and sub-headings within a section-typed in upper and lower case understood, flush left, followed by a period. Sub-sub headings should be italic. Articles should be written so that readers in different fields of acoustics can understand them easily. Manuscripts are only published if not normally exceeding twenty double-spaced text pages. If figures and illustrations are included then normally they should be restricted to no more than twelve-fifteen.

The first page of manuscripts should include on separate lines, the title of article, the names, of authors, affiliations and mailing addresses of authors in upper and lowers case. Do not include the author's title, position or degrees. Give an adequate post office address including pin or other postal code and the name of the city. An abstract of not more than 200 words should be included with each article. References should be numbered consecutively throughout the article with the number appearing as a superscript at the end of the sentence unless such placement causes ambiguity. The references should be grouped together, double spaced at the end of the article on a separate page. Footnotes are discouraged. Abbreviations and special terms must be defined if used.

EQUATIONS

Mathematical expressions should be typewritten as completely as possible. Equation should be numbered consecutively throughout the body of the article at the right hand margin in parentheses. Use letters and numbers for any equations in an appendix: Appendix A: (A1, (A2), etc. Equation numbers in the running text should be enclosed in parentheses, i.e., Eq. (1), Eqs. (1a) and (2a). Figures should be referred to as Fig. 1, Fig. 2, etc. Reference to table is in full: Table 1, Table 2, etc. Metric units should be used: the preferred from of metric unit is the System International (SI).

REFERENCES

The order and style of information differs slightly between periodical and book references and between published and unpublished references, depending on the available publication entries. A few examples are shown below.

Periodicals:

[1] S.R. Pride and M.W. Haartsen, 1996. Electroseismic wave properties, *J. Acoust. Soc. Am.*, **100** (3), 1301-1315.

[2] S.-H. Kim and I. Lee, 1996. Aeroelastic analysis of a flexible airfoil with free play non-linearity, *J. Sound Vib.*, **193** (4), 823-846.

Books:

[1] E.S. Skudzryk, 1968. *Simple and Comlex Vibratory Systems*, the Pennsylvania State University Press, London.

[2] E.H. Dowell, 1975. *Aeroelasticity of plates and shells*, Nordhoff, Leyden.

Others:

[1] J.N. Yang and A. Akbarpour, 1987. Technical Report NCEER-87-0007, Instantaneous Optimal Control Law For Tall Buildings Under Seismic Excitations.

SUMISSIONS

All materials from authors should be submitted in electronic form to the JASI Chief Editor: B. Chakraborty, CSIR - National Institute of Oceanography, Dona Paula, Goa-403 004, Tel: +91.832.2450.318, Fax: +91.832.2450.602,(e-mail: bishwajit@nio.org) For the item to be published in a given issue of a journal, the manuscript must reach the Chief Editor at least twelve week before the publication date.

SUMISSION OF ACCEPTED MANUSCRIPT

On acceptance, revised articles should be submitted in electronic form to the JASI Chief Editor (bishwajit@nio.org)